# Response inhibition in Premotor cortex corresponds to a complex reshuffle of the mesoscopic information network

**Giampiero Bardella[2,3], Valentina Giuffrida[1,2], Franco Giarrocco[1,2], Emiliano Brunamonti[2], Pierpaolo Pani[2], and Stefano Ferraina[2,*]**

[1]PhD Program in Behavioral Neuroscience, Sapienza University of Rome, Piazzale Aldo Moro 5, 00185, Rome, Italy
[2]Department of Physiology and Pharmacology, Sapienza University of Rome, Piazzale Aldo Moro 5, 00185, Rome, Italy
[3]INFN Sezione di Roma, Department of Physics, Sapienza University of Rome, Piazzale Aldo Moro 5, 00185, Rome, Italy
[*]corresponding author(s): Stefano Ferraina (stefano.ferraina@uniroma1.it)

## ABSTRACT

Despite recent works that have investigated functional and effective neural networks in animal models, the dynamics of information propagation among functional modules underneath cognitive control is still largely unknown. Here, we addressed the issue using Transfer Entropy and graph theory methods on mesoscopic neural activities recorded in the dorsal premotor cortex of rhesus monkeys. We focused our analysis on the decision time of a Stop-signal task looking for hallmarks in the network functional configuration, when the Stop signal is presented, that could influence the motor plan maturation. When comparing trials with successful inhibition to those with generated movement the nodes of the network resulted organized in four clusters, hierarchically arranged, and distinctively partaking in information transfer. Interestingly, the hierarchies and the strength of the information exchanged between clusters varied during the task, being distinct for generated movements and canceled ones and coupled with distinct levels of network complexity. Our results suggest that the premotor contribution to motor decisions involves a topological reorganization of information,with the intrinsic features of the network that delineate its behavioral functionalities.

**Keywords:** information theory | complexity | motor control | inhibition | networks | behavior

## 1 Introduction

The brain is a complex system composed of billions of neurons interacting at several spatial and temporal scales giving rise to networks organized in interconnected modules of varied sizes. At the small spatial scale, modules correspond to single neurons; at the large scale, modules correspond to specialized brain areas formed by many neurons. At the mesoscale, modules are neural populations of variable sizes, sometimes described as functional columns. Throughout the recent decades, neuroscience has attempted to characterize brain computations by relating neural activities to behavior. Understanding how network modules interact at the different scales and how information is shared and processed among parts is critical at all levels of investigation. Historically most approaches have relied on single unit activity to describe the neural correlates of behavior in discrete populations of neurons recorded in a single area[1–6] being able to characterize larger networks only occasionally[7,8]. Recent developments in microelectrode fabrication[9] have made it possible to record simultaneously from multiple channels and then investigate the dynamics of massive numbers of neurons and sites[10]. Nonetheless, the majority of studies focused on

single-unit activity (SUA) , and on the lower bands of the local field potentials (LFPs), which however indicate more the average synaptic input to the investigated area than the local spiking activity (for a review see[11]). Comparatively, few studies have looked at signals that sample the average spiking activity of the population of neurons in close proximity to the recording electrode (multiunit activity; MUA[12–15]). Such mesoscopic signals, more stable than SUA, can provide crucial information for investigating the local dynamics that enable brain function control.

In the arm motor domain, studies have indicated that neurons in the dorsal premotor (PMd) cortex of monkeys are engaged in motor control, as evidenced by modulation patterns of both SUA and mesoscopic signals (LFPs and MUA) obtained both at the single and population level[10,16–18]. Some studies have employed the Stop signal task[19], that requires actively inhibiting an upcoming movement upon presentation of a Stop signal, to investigate how neuronal activity in this area supports both movement generation and cancellation. According to these studies, neuronal activity in PMd is strongly related to both the generation and the suppression of an arm movement at different scales, from single neurons[20,21] to population of neurons[22] and local mesoscopic signals[14,23,24].

One of the proposed mechanisms suggests that arm movements are generated when neurons, following a Go signal, accumulate evidence up to a threshold, and inhibited when the accumulation is disrupted or postponed by a competing process triggered if a Stop signal is presented early enough after the Go signal. This view in which neurons work as stochastic accumulators stemmed from the analogy with the neural results in the oculomotor domain[25,26] and the original behavioral model[19] based on a competition between accumulating processes. Recently[23], it has been advanced the hypothesis that such evolution can be depicted as a dynamic in the state-space, in which movement generation and inhibition correspond to distinct neural trajectories hopping within specific subspaces. While these approaches have been fruitful in giving a mechanistic (or quasi- mechanistic) account of movement control, the issue can be tackled also from another perspective. For example, an alternative hypothesis is that movement generation necessitates the functional interactions of clusters of neurons to build networks that efficiently handle information locally and send information to other brain areas and/or the spinal cord (see Bassett & Sporns review[27]); thus one could also ask whether motor decisions are characterized by specific routings of information across mesoscale neuronal "components". Therefore, we studied the PMd's network dynamics using the MUA as a mesoscopic measure of spiking activity and implementing a combined information-theory and graph-theory approach to describe how the collective interaction of recorded modules is linked to motor decision-making. We demonstrated that in the behavioral epoch when decisions are made, mesoscopic modules may be classified into four distinct clusters that interact with one another and are organized hierarchically. Surprisingly, the hierarchical level of some of them, as well as the strength of interaction, differed before motor execution and when the animal successfully canceled the planned movement. Our results indicate that neurons in PMd have diverse opportunities to contribute to motor control at different spatial scales. In general, these findings support the idea of complexity being a core feature of the brain's ability in managing information at multiple levels of neural connection.

# 2 Materials and methods

## 2.1 Subjects

The study used two male rhesus macaque monkeys (Macaca mulatta; Monkeys P and C), weighing 9 and 9.5 kg, respectively. The animals' care, housing, surgical operations, and experiments were all in accordance with European (Directive 86/609/ECC and 2010/63/UE) and Italian (D.L. 116/92 and D.L. 26/2014) laws and were approved by the Italian Ministry of Health. The monkeys were housed in pairs and given cage enrichment. During the recording days, they were fed regular primate chow supplemented

with nuts and fresh fruits as needed, and they were given a daily water supply.

## 2.2 Apparatus and task

The monkeys were placed in a soundproof, dimly lighted chamber in front of an isoluminant black background with a brightness intensity of less than 0.1 cd/m2. They were shown stimuli on a 17-inch touchscreen panel with an LCD display with an 800 × 600 pixel resolution. CORTEX, a non-commercial software program available at http://www.nimh.gov.it, was used to control the presentation of stimuli and recording of behavioral responses. Figure 1 depicts the overall task, which our group first described as a stop-signal reaching task[20]. The central target (CT), a red circle with a diameter of 1.9 cm, was displayed at the start of each trial. The CT had to be reached by the monkeys to initiate the trial. A peripheral target (PT) randomly appeared on the left or right side of the screen after a variable holding duration of 400–900 ms, in steps of 100 ms. At the end of the holding period the CT vanished, signaling a Go signal. In the Go trials, the monkeys had to reach and hold on the PT for a range of 400–800 ms, in steps of 100 ms, to get a juice reward. The time between the presentation of the Go signal and the beginning of the hand movement was used to compute the reaction time (RT). The sequence of events in Stop trials was the same as in Go trials until the Go signal. The CT reappeared as the Stop signal after a variable delay known as the Stop signal delay (SSD), and the monkeys had to hold the CT until the end of the trial, which was between 800-1000 ms, to get the reward for a correct Stop trial. If the monkey removed its hand before the trial ended, it was considered an incorrect response for a Stop trial. For both correct Stop and correct Go trials, the same amount of juice was provided. The inter-trial interval was set at 800 milliseconds. Stop trials accounted for approximately 25% of all Monkey P trials and 32% of Monkey C trials. White rings around the central target provided input for the animals to signify touch. A staircase tracking approach was utilized to determine the duration of the SSDs, to obtain a success rate of roughly 50% in Stop trials. The SSD rose by 100 ms in the succeeding Stop trial if the monkey successfully withheld the movement, but it reduced by 100 ms if the monkey failed to cancel the response.

## 2.3 Behavioral considerations

The stop-signal reaching task allows for the calculation of the Stop signal reaction time (SSRT), which is often recognised as a metric of efficiency in movement suppression. The race model[19] is used to describe the behavior in the Stop trials, which involves two stochastic processes racing towards a threshold: the GO process, which is triggered by the Go signal and whose duration is represented by the RT, and the STOP process, whose duration must be derived. If the GO process wins the race against the STOP process, the movement is generated (resulting in wrong Stop trials). If instead the STOP process prevails, the movement is restrained (resulting in correct Stop trials). We may estimate the SSRT using the race model by considering the duration of the GO process, the probability of response, and the stop-signal delays (SSDs). To estimate the SSRT, we used the integration approach, which has been demonstrated to be the most trustworthy[28]. This technique considers the fact that there is a certain probability of response [p(response)] for a given SSD in Stop trials. The longer the SSD, the higher the p(response), indicating a higher likelihood of a wrong Stop trial. By integrating p(response) over the distribution of Go trials, we can derive the nth value Go RT. Subtraction of the SSD from the nth Go RT yields the SSRT. To visualize the procedure imagine an SSD where p (response) is exactly 0.5. For such SSD, the Go and Stop process would have the same probability of winning the race, meaning that the Stop and Go processes will both reach the threshold at the same time (from a probabilistic point of view). It should be emphasized that the completion times of the Stop and Go processes are, respectively, the end of the SSRT and the end of the RT (i.e., the beginning of movement). In the current investigation, we compared the evolution of brain activity during movement preparation in the Go trials to the inhibitory effect of the Stop signal in correct

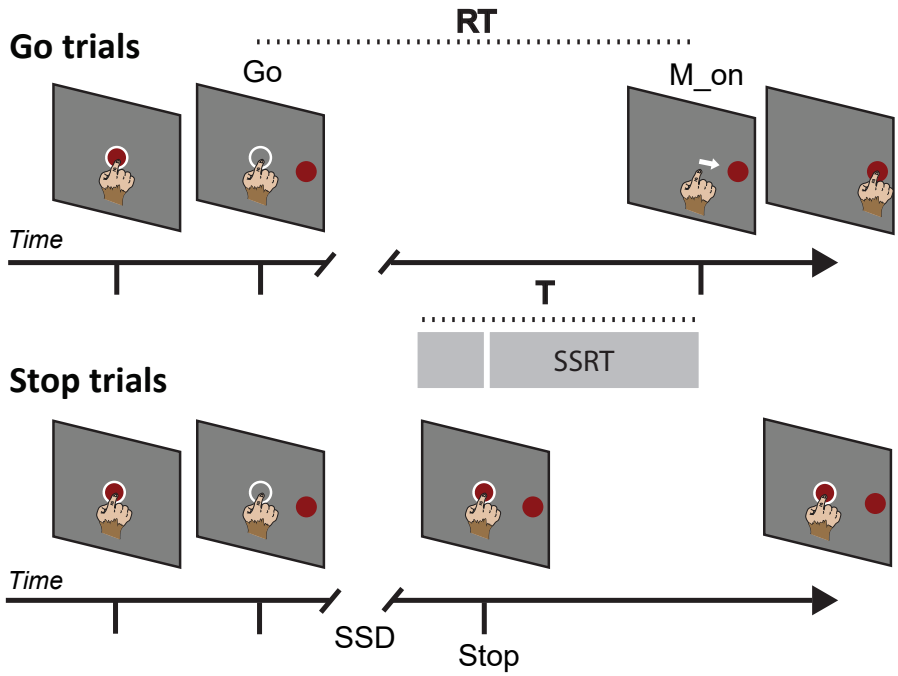


**Figure 1. Sequence of Behavioral events characterizing the task**. Go and Stop trials were randomly intermixed during each session. The epoch (T) of neural analysis is shown as a grey bar for both trials. RT, reaction time; SSD, Stop signal delay; SSRT, Stop signal reaction time. White circles are feedbacks for the touch provided to the animals. Go: time of Go signal appearance; Stop: time of Stop signal appearance. M_on: time for Movement onset.

Stop trials. To make this comparison effective, we considered an epoch before movement generation in Go trials and an epoch starting before the Stop signal and ending at the conclusion of the Stop process (SSRT duration) in correct Stop trials (see below). When adding wrong Stop trials in the analysis, we aligned neural activities to the beginning of movement. Because different SSDs were used in separate recording sessions, and because RT distributions also varied, resulting in varying SSRTs across sessions, we chose an epoch that could contain all estimated SSRTs in the various sessions (see Table S1). We decided for a duration of 400 ms for the epoch of analysis (Fig.1, epoch T, gray bar). In Stop trials, we verified that the epoch T did not include the Go signal when short SSDs were employed.

## 2.4 Extraction and processing of neuronal data

In the left PMd, a multielectrode array (Blackrock Microsystems, Salt Lake City) with 96 electrodes spaced at 0.4 mm was surgically implanted. After opening the dura, the arcuate sulcus and precentral dimple were employed as reference. We recorded the raw signal using a Tucker Davis Technologies (Alachua, FL) system, sampling at 24.4 kHz. As a measure of neuronal activity at the population level, local MUA was extracted offline from the raw signal. This was accomplished by computing the time-varying power spectra $P(\omega, t)$ from the signal's short-time Fourier transform in 5-ms sliding windows, as described in Mattia et al.[14]. Relative spectra $R(\omega, t)$ were obtained normalizing $P(\omega, t)$ by their average $P_{ref}(\omega)$ across a fixed window (30 minutes) for the entire recording. Thus, the average $R(\omega, t)$ across the $\omega/2\pi$ band $[0.2, 1.5]$ $kHz$ represents the spectral estimated MUA, our mesoscopic measure of spiking activity. As explained in Mattia et al.[14], such estimation relies on two hypotheses. The first is that high $\omega$ components

of the raw signal result from the convolution of firing rates $\nu$(t) of neurons that are close to the electrode tip with a stereotypical single-unit waveform. The Fourier transform K($\omega$) of such an unknown waveform is canceled out in R($\omega$, t), which is therefore a good approximation of the ratio of firing rate spectra $|\nu(\omega,t)|^2 / |\nu_{\text{ref}}(\omega)|^2$. The second is that high $\omega$ power $|\nu(\omega,t)|^2$ is proportional to the firing rate $\nu$(t) itself[29], such that our estimated spiking activity is proportional to $\nu$(t). As a last step, logarithmically scaled MUAs were smoothed by a moving average (40 ms sliding window, 5ms step). Previously, similar methods for obtaining the aggregate spiking activity of a population of neurons in the vicinity of the electrode without spike detection were used[12,14,30,31].

### 2.5 Quantifying information dynamics with Transfer Entropy

Based on the MUA obtained from each electrode site, we used multivariate Transfer Entropy (TE)[32,33] to infer patterns of local information dynamics in the PMd, as well as the directed functional relationship between different neural populations (modules) and the collective state of the information flow through the PMd network at the time of the motor decision. TE, particularly in its multivariate formulation, has been shown to be more accurate than other measures[34,35], and it is recognised to also capture possible nonlinear interactions in system dynamics without assuming any generative model. Furthermore, TE is gaining popularity in neuroscience, with a blooming literature[36–45]. Given an ensemble of M time series, the multivariate information transfer from a time series $X$ to a time series $Y$, conditioned to the remaining $Z_{k=1,..,M-2}$ time series, can be quantified considering the present values of $Y$ and the past values of both $X$ and the Z through[36,46,47]:

$$TE_{X\to Y\,|\,Z} = H(Y_n \mid Y_n^-, Z_n^-) - H(Y_n \mid Y_n^-, X_n^-, Z_n^-)\ , \tag{1}$$

where $Y_n$ is the vector that represent the present state $n$ of Y, $X_n^- = [X_{n-1}, X_{n-2}, ...]$, $Y_n^- = [Y_{n-1}, Y_{n-2}, ...]$ and $Z_n^- = [Z_{n-1}, Z_{n-2}, ...]$ are the vectors that represent the past of X, Y and Z respectively. The vertical bar stands for conditional probability, e.g. $H(Y_n \mid Y_n^-, Z_n^-)$ is the entropy of the present state of Y conditioned to the knowledge of the past of Y and to the past of the remaining Z. $H$ is the Shannon entropy[48], which in the case of $Y$ is given by:

$$H(Y_n) = -\sum_n P(Y_n)\, log P(Y_n)\ , \tag{2}$$

where P indicates the probability density. Hence, using equation 2 expression 1 becomes

$$TE_{X\to Y\,|\,Z} = -\sum_n P(Y_n, Y_n^-, X_n^-, Z_n^-)\, log \frac{P(Y_n \mid Y_n^-, X_n^-, Z_n^-)}{P(Y_n \mid Y_n^-, Z_n^-)} \tag{3}$$

TE is $\geq 0$ and, in this formulation, increases if the history of $X$ gives more information about the present of $Y$ than the past of $Y$ or any other series contained in Z. Because the past of $X$ is used to predict the present of Y, TE is not symmetric (i.e. $TE_{X\to Y} \neq TE_{Y\to X}$) and defines an information transfer direction, which corresponds to a driver-to-target causal relationship. Approximating the vectors that represent the time series' history, a process known as *embedding*, is a critical difficulty in estimating TE. The optimal embedding should include just the $X_n^-$, $Y_n^-$ and $Z_n^-$ components that are most informative in describing $Y_n$. Montalto and colleagues[46] have discussed numerous approaches for embedding and assessing probability distribution functions required to compute the entropy terms. We used a non-uniform embedding scheme[49]

and computed $H$ with kernel estimators[1] In short, the embedding approach we adopted selects components from the system's past based on highest relevance and minimum redundancy requirements. Maximum relevance means the most significant predicted information components. Non-uniform embedding selects informative components from the past of X, Y, and Z, gradually removing non-informative terms. The maximum number of prior values, or maximum lag $l$, considered to initialise the pruning is predetermined at the start of the procedure. The statistical significance is progressively assessed by cycling through the past components (up to $l$) and comparing them with a null distribution constructed from empirical data using a randomization procedure[46]. If the components of the past of X, Y, and Z reach a certain amount of $\alpha$, they are considered statistically significant. We obtained the null distribution by executing 300 random shuffles of empirical values while keeping $\alpha$constant at 0.01. Non-uniform embedding is a more reliable[36] alternative to uniform embedding, which would choose the previous values $X_n^-$, $Y_n^-$ and $Z_n^-$ a priori and separately for each time series[46]. To estimate the probability densities required for the computation of $H$ the Kernel estimator was used. This reconstructs the probability distribution at each data point by weighing the distance from the reference point to any other point in the time series. This method uses a local exploration of the state space, making it more robust to inaccurate estimations compared to other approaches[36]. Thus, if the non-uniform embedding procedure selects at least one component from the past, the resulting $TE_{X \to Y \mid Z}$ is > 0 and statistically significant. If none of the components of the past provide statically significant information about the target the $TE_{X \to Y \mid Z}$ is deemed to be non-significant and equal to 0[46]. To avoid any further bias in the selection of the past values we initially fixed $l$=50 ms, but, as expected, only a recent past was selected by the procedure, in line with similar studies[37,51–53]. Indeed, for each MUA time series, a past no older than 10ms for each $n$ of equation 2 was ever selected by the optimal embedding procedure. This is consistent with prior research, which indicates that neuronal populations in the cortex typically create causal interactions and exchange information within a time range of 1 to 20 ms[54–56]. Within this framework, we built single-trial information transfer networks for each behavioural condition of each recording session by customising some Matlab MUTE[46] toolbox functions. Because the application of information theory techniques in neuroscience is still in its early stages, it is worth briefly examining their usage on invasive neurophysiological data. Gomez-Herrero[57], Bossomaier[43], Wibral[40], Newman[45] and colleagues have published technical discussions on this topic. Timme and Lapish landmark review[58] is recommended for a full treatment of the essential themes in the field. The main assumption made by experimenters using information theory techniques to brain data, as summarised in the latter, concerns the stationarity of the neural processes under examination. Stationarity of a process means that the probability density function that generates the observable variables does not vary over time, and each observation contributes to the same probability distribution. In practice, this translates into viewing the experimental trials as multiple realizations of the same underlying mechanism. In other words, assuming stationarity implies that each observed realisation helps to define the same underlying probability distribution[37], which finally becomes stable over time, i.e., the lifetime of the experiment. In a behavioural neurophysiology experiment, the observations correspond to neural activity values, the realisations to repeated trials, and the probability distribution to the probability distribution characteristic of the investigated neural process that is supposed to generate the observed behaviour. It is critical to remember that in any experimental paradigm, this distribution is not known a *a priori* and is almost never accessible, in contrast to any theoretical study in which time series are generated based on many repetitions of processes whose analytical details are known. Furthermore, as Wollstadt[37] and colleagues note, stationarity does not imply a flat variability across realisations, and some variance is

[1]For a complete description of embedding methods and estimators for computing $H$, refer to the works of Faes and colleagues and the references cited therein[47,49,50].

expected, reflecting the natural fluctuation of the underlying (unknown) probability distribution. For these reasons, when an experiment has a multi-trial structure, stationarity over realizations is assumed by default, provided that no slow drifts or trends affect the signal, being the latter one of the non-stationarity factors that most impinge on a correct estimation of TE[36]. These could arise during training or in an experiment that encourages learning[37]. Indeed, these are the most prevalent scenarios in which the probability distribution of both the brain signal and the behavioural parameters changes over time by definition. As a first step in using TE on our data, we analysed the single-trials MUA profiles of each module for each recording session for both animals. Our estimate of MUA is baseline corrected (see section 2.4) so any potentially distorting slow trends are eliminated. Furthermore, to remove noisy outliers from our data, we excluded from the analysis the trials for which the MUAs showed peaks with an amplitude that exceeded the average of the activity by 2 standard deviations in any of the time bins of the epoch of interest and for over 80% of the channels[24] (which accounted for less than 2% of the total number of trials). This ensures that artifacts caused by non-physiological peaks and/or segments of oscillations of high variance in the time series are excluded from the analysis. These non-stationary artefacts, as detailed by Xiong and colleagues[36], are among those that have the most impact on trustworthy TE estimation. If present, they could influence the probability distributions in equation 3 in such a way that outliers would dominate most of the signal variance, significantly biasing the estimation of the temporal link between the current and past states of the time series. As previously stated, the kernel estimator is particularly useful in this aspect since it removes any potential residual dependency of the estimated TE on the signal's variance through tighter local exploration of the state space.

## 2.6 Graph theoretical analysis

For each behavioural condition (Go, correct and wrong Stop trials) for both monkeys in the epoch T, we first obtained a single-trial $TE$ matrix. Assuming that the nodes are single modules (discrete neuronal populations producing MUAs) and the weighted edges are the $TE$ values, we interpreted the $TE$ matrix as the adjacency matrix of a directed weighted network. We disregarded the main diagonal of the matrix thus excluding self-loops from the networks. Then, we aggregated the trials of the same condition for each recording session to get the appropriate trial-averaged matrices on which we applied percolation[24,59–69]. During percolation, the iterative pruning of links based on their weights is used to monitor the stability of network topology. Percolation was used in this work for two reasons. First, we used percolation to remove weaker links that were influenced by statistical noise caused by trial averaging. This method served as a fine-grained cleaning tool for false positives TE values, as some non-zero TE measurements may arise due to the experimenter's limited sample size, even though there is no direct link between the variables[43]. After the bias-corrected estimators (discussed in Section 2.5), our pipeline included percolation analysis as a topology-based and data-driven way to solving this issue. This remove the hindrance of optimal thresholding, a common problem when dealing with connectivity matrices[24,60,63], without the need for computationally intractable full error-correction inference of each link at the whole network level. Second, percolation was used to analyse the global organisation of the network and how hierarchical information flow between nodes shape the complexity of network topology. Percolation analysis produces a curve that plots the size of the largest connected component of the network against link weights. Because the networks we studied were weighted and directed, we used percolation analysis on the giant strongly connected component[70,71] (GSCC). Very briefly, a GSCC is a subgraph in which every vertex is reachable from every other vertex following the direction of the links. For simplicity, in the Results we will refer to the threshold at which the fragmentation of the largest component begins (formally, the percolation threshold) as the "descent point" of the curves. Such threshold achieves the best balance between the removal of spurious links and the consequent loss of information potentially

encoded in those links[62,67]. The power of percolation lies in displaying the stepped pattern of the curve, which suggests a transitory stable network architecture composed of hierarchical connections between nodes. A steeper curve with no or few leaps, on the other hand, indicates a single incipient component that dominates the network and fragments swiftly in fewer or a single step. Thus, the process naturally discloses simultaneously both network robustness and its hierarchical self-organization. In addition, the percolation threshold identifies the level of complexity of the network: a higher threshold means a stronger component; a stronger component means that more links need to be removed to fragment it; more links implies more paths between nodes and thus higher complexity. Thus, we could estimate the complexity of information flow-paths within the network (under different behavioural conditions) by evaluating fragmentation at higher thresholds. Please, refer to our prior studies and to Gallos and colleagues' work[24,60,61] for additional details on the percolation analysis applied to brain networks.

On each trial-averaged matrix, we measured the Vertex Degree (VD), which is the number of links to each node $i$:

$$VD_{\mathrm{i}} = \sum_{j=1}^{N} a_{\mathrm{ij}} \ , \tag{4}$$

where $a_{\mathrm{ij}}$ is the generic entry of the adjacency matrix and N is the number of nodes. In directed networks one can distinguish between in-degree (the number on inward links) and out-degree (the number of outward links).For each behavioural condition of each recording session, we estimated the probability distribution of both VDs (i.e., the in/out-degree distribution) for both animals. If the variance of the degree distribution is significantly larger than its mean, tails in the distribution arise and network hubs are found. Hubs are thus nodes that significantly exceed the average degree of the network (here we used mean $\pm$ 2 standard deviations of the out-degree distributions[72–74]). After hubs were identified, we sorted nodes into clusters to better understand their contribution to information sharing in the network. We labelled the nodes based on the two possible outputs of the motor behaviours studied in the task, namely movement generation (correct Go trials) and movement inhibition (correct Stop trials). In our paradigm, TE values represent the strength of connections between nodes, and clusters are created depending on how much information nodes spread within the local PMd network and during certain behavioural conditions. We customized an interaction measure $I$ using the following equation to summarise the overall quantity of information exchanged between clusters:

$$I_{\mathrm{ij}}{}^{(\mathrm{m,n})} = \rho \sum_{i}^{M} \sum_{j}^{M} \sum_{(m,n)} TE_{C_{\mathrm{i}}{}^{\mathrm{m}} \rightarrow C_{\mathrm{j}}{}^{\mathrm{n}}} \ , \tag{5}$$

where C is the module's cluster, M is the number of clusters (M=4) and m and n run over the all possible combinations of nodes within each cluster. $\rho = \frac{1}{dim\,(C_{\mathrm{i}})}$ is a normalization factor that accounts for the heterogeneous number of nodes within each of the clusters. Thus, our $\mathrm{I_{ij}}$ is equivalent to a normalised node strength computed on the graph formed by the 4 clusters. The strength of a node in a weighted graph is the total of the weights of the links that connect to the node. As a result, the values and directions of I reflect the cluster's location in the network communication hierarchy. We enclosed all of the interactions defined by the empirical TE matrix in a 4x4 matrix that represented an interaction network, with each node representing a functional cluster. $I$ was calculated for each recording session and behavioural condition, and the sessions-averaged (mean $\pm$ SEM) element $\overline{I}_{\mathrm{ij}}$ was derived (see Figure 7 and supplementary Table S3 and S4).

#### 2.6.1 A null model

We built a null network model to assess the statistical significance of the results beyond what was attained by the randomization approach used in the TE computations. As noted in a recent work[75], selecting a suitable null model remains a thorny issue in network and complex systems science. When analysing real-world networks, such as those examined in this study, it is common practice to look for characteristics that deviate from the null hypothesis being likely that such variations contain information about the network's features. In this study, we drew our conclusions regarding the PMd information network exclusively from brain activity in a data-driven fashion, with no external constraints. Thus, we investigated whether the results could be explained by the distribution of MUA values and the dimensions of the time series. In the latter situation, however, our sample size was far from the reliability limits described in the literature for comparable systems[42,58]. Nonetheless, we added it as an additional control in the null model. We constructed a synthetic pool of N time series with the same length as the empirical ones (with N number of recording channels) for each trial of each behavioural condition and recording session by randomly sampling from the empirical MUA distribution. The trial-averaged TE matrix for each synthetic pool was then computed. This is the most general approach because no assumptions are made about the connection patterns and weight distributions of the synthetic networks. Finally, we compared our empirical metrics to the results of the 500 randomizations ensemble. The degree distributions of the experimental networks had a variance that was at least one order of magnitude larger than that of the networks produced from the MUA distribution, despite having comparable mean values (see supplementary figure S5).

# 3 Results

Table S1 shows behavioral data from 21 recording sessions, 12 from Monkey P and 9 from Monkey C. We ensured that the race model's fundamental premise was followed in all sessions. To be more specific, the Go process in the Stop trials must be the same as the Go process in the Go trials to compute the SSRT. This assumption is usually satisfied by showing that RTs in wrong Stop trials are shorter than RTs in Go trials, as shown in Table S1. This indicates that all trials are drawn from the same distribution of RTs. Across all sessions, the average RT for Monkey P was 656 ms (SD = 129 ms) and 632 ms (SD = 119 ms) for Monkey C. The average SSRT was 217 ms (SD = 34 ms) for Monkey P and 213 ms (SD = 26 ms) for Monkey C.

## 3.1 Neural activity express an evident contribution to motor control when examined at the single site level

Fig 2 illustrates the time course of the average MUA obtained from each cortical site separately during Go trials (dark green traces), correct Stop trials (red traces), and wrong Stop trials (dark blue traces) during the time (epoch T in Figure 1) preceding the movement onset (in Go trials and wrong Stop trials) or the end of the SSRT (in correct Stop trials) for one example session of Monkey P (S6 of Table S1). The activity in the wrong Stop trials appears to be indistinguishable from the activity in the Go trials for all sites. In contrast, the presentation of the Stop signal (red vertical line) and the effective cancellation of movement produce a distinct pattern in many of the locations, with the spiking activity modulated (increasing or decreasing) compared to the activity during movement generation. We found, in this session, a significant difference between the Go and correct Stop conditions in 78% of the recording sites. Conversely, there was no significant difference in spiking activity between the Go and wrong Stop trials at any of the sites. A similar trend was found in all recording sessions (Table S1), confirming previous findings on the role of PMd in inhibitory motor control and the relevance of the epoch of analysis in motor decisions in Stop trials[20,22–24,76–79]. This level of analysis, however, does not provide information on how the nodes in the

investigated network interacted.

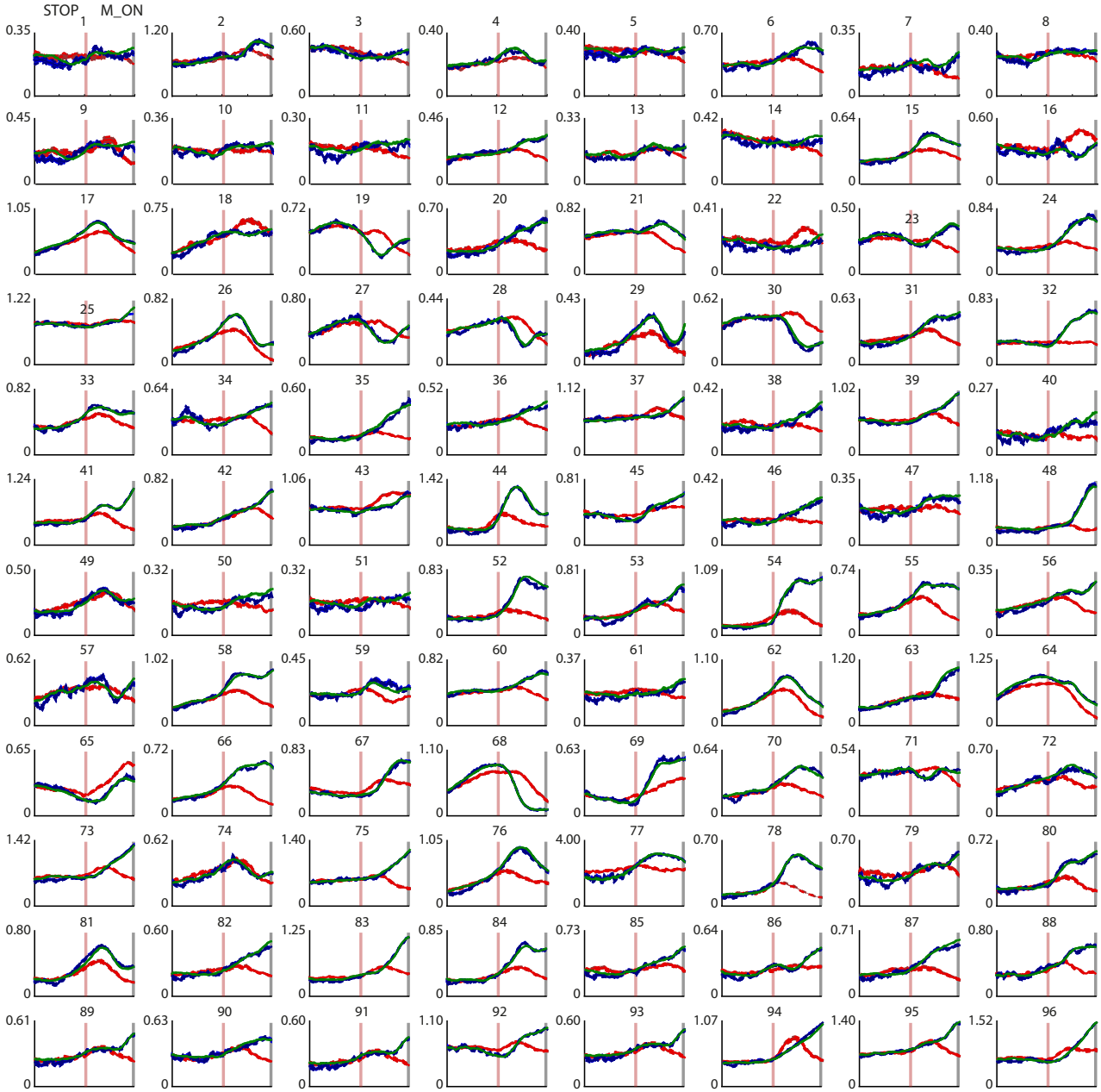


**Figure 2. Neuronal activity modulation in different trials type.** Neuronal MUAs (mean ± SEM) in the epoch T for the three behavioural conditions for all recording sites (modules) of S6 of Monkey P. Dark green traces show the average activity during Go trials aligned to the movement onset (gray vertical line). Dark blue traces show the average activity during wrong Stop trials aligned to the movement onset (gray vertical line). Red traces show the average activity during correct Stop trials aligned to the Stop signal presentation (light red vertical line) and plotted until the end of the SSRT. Each neuronal MUA is baseline corrected. For each plot the Y axes are units of MUA while the X axes mark the time during the epoch T; ticks in the first top left panel are every 100 ms. (**STOP**: Stop Signal appearance; **M_ON**: movement onset).

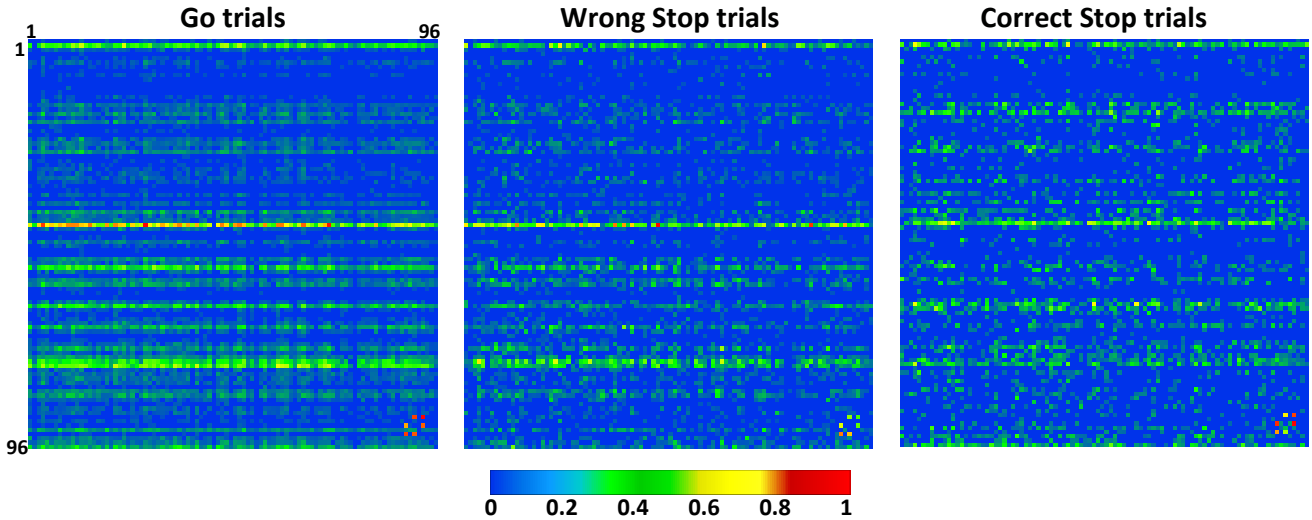


**Figure 3. Average TE matrices** of Go, wrong and correct Stop trials for data in Fig.2. Each entry of the matrix is color-coded according to the corresponding average TE value across trials. Statistically significant driver→ target relationships correspond to TE values > 0 for the pair of modules considered. Here, for graphical purposes only, TE is normalized to the maximum across behavioural conditions so to obtain TE $\in [0,1]$. The color bar indicates the normalized values of TE.

### 3.2 Hierarchical organization of Information transfer in the PMd network

Fig.3 shows the TE matrix for each trial type derived from the data provided in Figure 2. A TE > 0 implies that the pair of recording sites under consideration has a statistically significant driver → target relation. The dense horizontal stripes that change between Go, correct, and wrongStop trials suggest that, depending on the behavioral situation, a few of the sites might influence the activity of many others during the epoch where the motor choice is taken. We used graph-based measurements to provide a detailed description of the differences in information transmission at the network level (i.e., the network topology) for both the example session and all other sessions. In this picture, any recording location is represented as a network node, and any significant TE value is a link between nodes. As a first step, we calculated the vertex degree (VD) for the average thresholded networks, as determined by percolation analysis after removing the noisiest links[24,60,62,63,67] (see Section 2.6). A high VD score indicates that some modules are functionally related to many others and serve as hubs. Hubs only appeared in the out-degree ($VD_{out}$) distributions (see Supplementary Figure S1). In each session, we labeled the nodes based on the behavioral condition in which they assumed the role of hub. Specifically, nodes were classified as **C_3**, which resulted as hubs in both Go and correct Stop trials, or **C_1** or **C_2**, which appeared only in trials where the movement was generated or successfully canceled, respectively. **C_4** are all the remaining nodes that have never served as hubs. **C_4** are all the remaining nodes that have never served as hubs. Strikingly, no new hubs were found when movements were incorrectly inhibited after a Stop signal (wrong Stop trials), implying that the same neuronal clusters as in Go and correct Stop trials are recruited in trials where errors occur. The percentage of hubs belonging to each cluster throughout all sessions is shown in Table 1. In both animals, more than 70% of the nodes were acted as **C_4 cluster**. Approximately 10% of the remaining hubs acted as **C_3**, while the rest acted as **C_1** or **C_2**, depending on the behavioral conditions. One might wonder if there is any internal hierarchy between the clusters, specifically whether the $VD_{out}$ of the nodes in a cluster changes selectively depending on the behavioral conditions. To answer, we kept the cluster label assigned by the aforementioned process and looked at how the $VD_{out}$ of the nodes in each cluster differed across

trial types. **C_3** consistently exhibited the highest $VD_{out}$ values across all three behavioral conditions across all sessions (see Table S2; see Supplementary Figure S2 for other examples of individual sessions), indicating that they are the primary hubs for spreading information (Kruskal-Wallis, p 0.01, Bonferroni corrected for multiple comparisons).

| **Clusters Composition** | |
|---|---|
| **Monkey P** | $N = 96$ |
| **Cluster** | $\boldsymbol{\mu \pm SEM}$ |
| cluster_1 | $9.3 \pm 1.06$ |
| cluster_2 | $3.6 \pm 1.4$ |
| cluster_3 | $11.8 \pm 1.6$ |
| cluster_4 | $71.3 \pm 2.3$ |
| **Monkey C** | $N = 96$ |
| **Cluster** | $\boldsymbol{\mu \pm SEM}$ |
| cluster_1 | $7.4 \pm 0.8$ |
| cluster_2 | $4.1 \pm 0.6$ |
| cluster_3 | $9.4 \pm 1.1$ |
| cluster_4 | $75.0 \pm 1.8$ |

**Table 1. Clusters composition**. For each monkey the composition of clusters averaged (mean $\pm$ SEM) over recording sessions is reported. $N$ is the number of modules available.

Thus, **C_3** are at the highest hierarchical level in the network because they regulate information transfer regardless of whether the decision is to move or stop. The **C_1** and **C_2**, on the other hand, demonstrate distinct levels of engagement, with lower $VD_{out}$ values in Go and correct Stop trials, respectively, showing that their hierarchical role shift based on the type of motor choice being processed. In Go trials, the **C_2** had lower $VD_{out}$ values than the **C_1**, whereas in correct Stop trials, the **C_1** had lower $VD_{out}$ values than the **C_2**. Interestingly, the **C_1** had larger $VD_{out}$ values during wrong Stop trials than during correct Stop trials, whereas the **C_2** had the opposite (Kruskal-Wallis, $p < 0.01$ Bonferroni corrected for multiple comparisons). This reveals that during wrong Stop trials, the neuronal processing of information is midway between Go and correct Stop trials, but more comparable to Go trials. The presence of four distinct clusters indicates that the PMd information network's intrinsic composition is heterogeneous, with some nodes serving as driving hubs only in relation to a specific behavioral outcome: executing or withholding the planned movement. Furthermore, the variation in $VD_{out}$ values across trial types suggests that the network configuration underlying information transmission is fine-grained and changes depending on the decision that leads to a specific behavioral output. The topology of the PMd network for data in Fig.3 is depicted in Fig.4, highlighting the relevant features of the hubs that change between conditions **C_1** and **C_2**; for networks including also the **C_3** see Figure S2 in the supplementary materials).

Each link in the graph represents a significant TE value (i.e., a non-zero entry in the TE matrix) between the corresponding modules, and the number of outgoing connections of each module reflects its $VD_{out}$ value, i.e., the number of modules on which it acts as a driver. Modules are labeled according to their cluster, and links are coloured according to the source node (e.g., an arrow is green if it originates from a **C_1**). The centralized organization of the information network is largely observable in Go trials (and to a lesser extent in wrong Stop trials), corroborating previous studies that showed how such functional

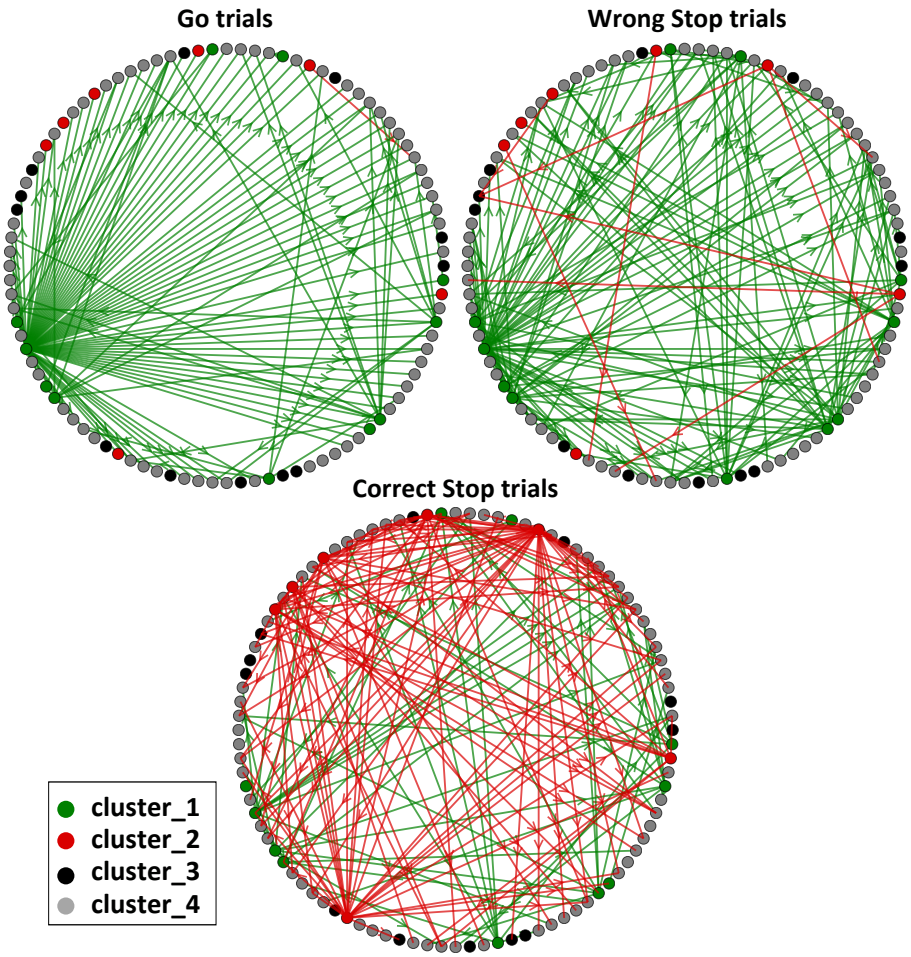


**Figure 4.** Information network of Go, wrong, and correct Stop trials. Data from the same recording session of Fig.2 and Fig.3. Each link is colour coded accordingly to the cluster its source node belongs to. Nodes with a high number of outgoing connections are the information-spreaders hubs. Here, for illustrative purposes and to better highlight the differences between behavioural conditions, the links of the C_3 nodes are removed and for each network only the 20% of the strongest links are shown (for the complete version including the C_3 see supplementary Figure S3). The coordinates of each node on the circle are preserved across behavioral conditions.

conditions facilitate movement generation[24]. Fig.4 (and Supplementary Figures S3 and S4) show how the **C_1** act as hubs during Go and wrong Stop trials, whereas the **C_2** appear as major nodes of information propagation during correct Stop trials only . Furthermore, the optimal centralized transmission present during Go trials is disrupted during correct Stop trials. The link arrangement is more complex and compounded , with more intersections and less directness as compared to Go trials. As a result, the network retains its core features (the existence of hubs) across trials, but the way these elements are deployed varies depending on the needed behavioral control.

### 3.3 The organization of the PMd network shifts towards higher complexity in Stop trials

According to the results described so far, the contribution of each cluster to the overall network topology varies across behavioral conditions, particularly in terms of the number of links provided by each node when acting as a hub. To better understand the hierarchical relationships between the clusters and how the

information they manage relates to the overall network organization, we analyzed the $VD_{out}$ as a function of TE. This involved tracking the changes in $VD_{out}$ of each cluster as the percolation process progressed. This step compares the resilience of the information carried by each cluster to the information spread by the others, yielding a global and weighted validation of the hierarchical relationships found with $VD_{out}$. Indeed, we expect a cluster that is functionally relevant to a specific behavioral condition to have not only a large number of connections (a high $VD_{out}$ value) but also for many of these connections to have a high and robust information content (high $VD_{out}$ for high TE values).

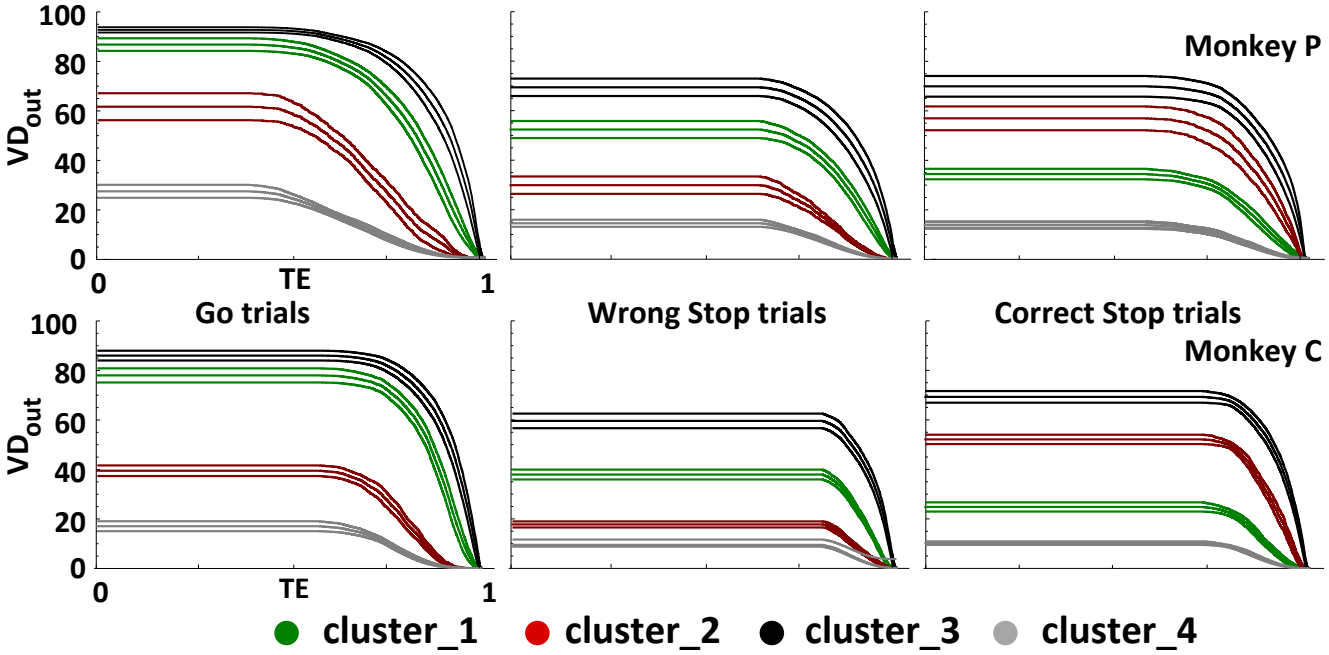


**Figure 5. Clusters robustness analysis.** Robustness is inferred by monitoring the evolution of $VD_{out}$ (y axis) as a function of the information processed (TE, x axis). Panels show the robustness curves averaged (mean $\pm$ SEM) over recording sessions compared between clusters and across behavioural conditions. Curves are colour coded accordingly to the corresponding cluster as in Fig.4.

.

The robustness analysis results are shown in Fig. 5 as the average of all recorded sessions of each animal. The analysis confirmed the **C_3** as the highest hierarchical level cluster in all three behavioral conditions, with the highest persistent values of $VD_{out}$ as a function of the amount of information processed, indicating that the C_3 cluster had the most links with high and robust information content. The **C_1** and **C_2**, on the other hand, were placed between the **C_3** and the **C_4**, and their hierarchical level changed depending on the trial type. Thus, the figure suggests that the network's structure is similar in both wrong and correct Stop trials at the global level. To investigate the complexities conveyed by the network under the three behavioral settings, we inspected the percolation curves as a function of the network's GSCC (see Section 2.6). Figure 6 shows that the percolation curves of the Go trials follow a different route from those of the Stop trials (whether correct or wrong) and the null model for all sessions. The curves for the Go trials begin their descent at lower TE values than the others and have a more stepped pattern (normalized among conditions). Therefore, the Go trials show fewer paths belonging to the giant component itself, with most links with high information content heading outwards to the rest of the network. This is a symptom of an ideal network setup with more direct and organized communication than in the Stop trials. One important implication is that in the Go trials the number of redundant links is very low.

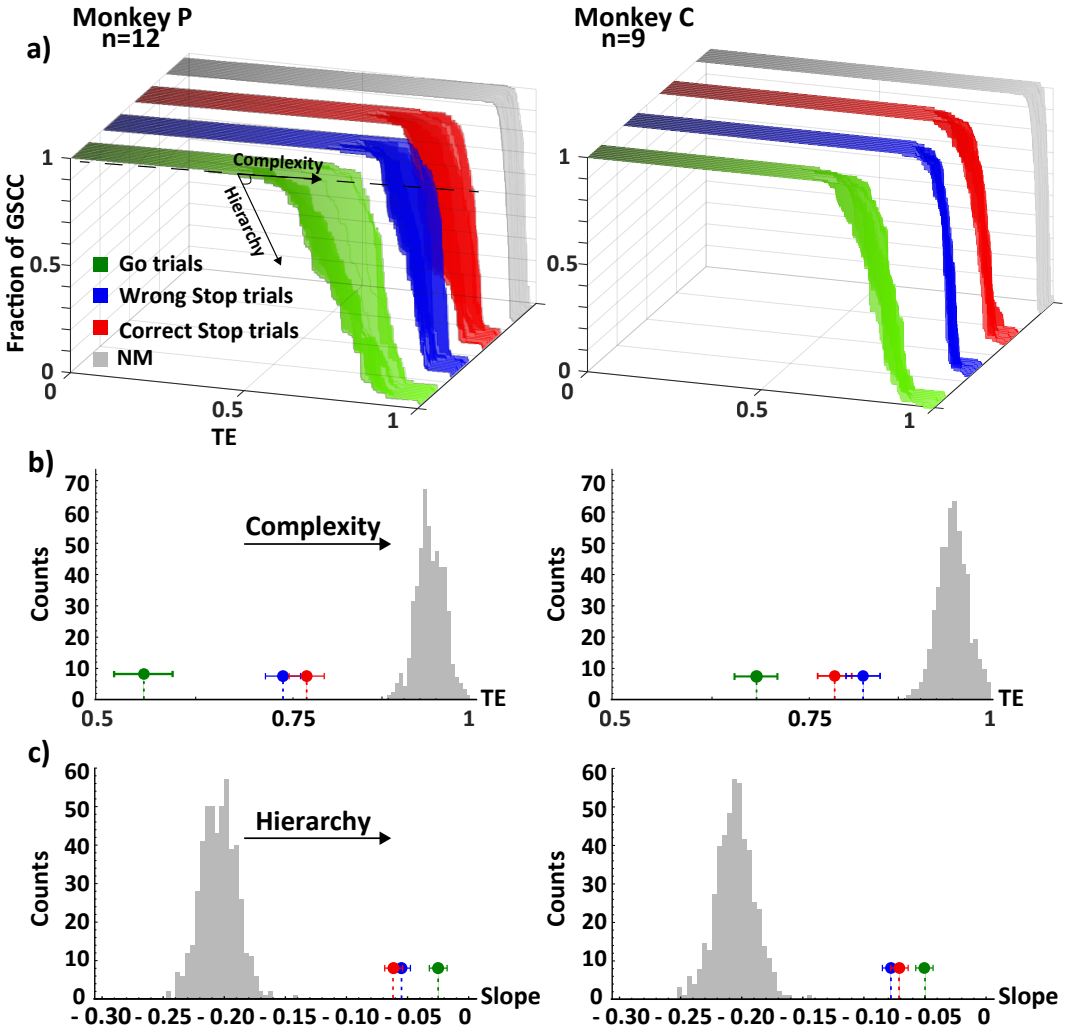


**Figure 6. Percolation analysis. a:** percolation curves over recording sessions compared across behavioural conditions and vs the null model for both animals. Each curve is a recording session. As sketched, the level of complexity of the underlying networks increases travelling the curves from left to right, whereas the hierarchy can be explored climbing down the steps of the curves (the fraction of GSCC, z axis), measured in unit of information (TE, x axis). **b:** comparison between the point of descent between behavioral conditions (mean $\pm$ SEM) and against the null model distribution. **c:** comparison between the measured slopes between behavioral conditions (mean $\pm$ SEM) and against the null model distribution. Stop trials resulted more complex and less hierarchical than Go trials while having comparable values between themselves (Kruskal-Wallis, $p < 0.01$ Bonferroni corrected for multiple comparisons). In all panels, for simplicity and homogeneity, TE is reported normalized to its maximum so to obtain TE $\in [0, 1]$. The null distribution is obtained from 500 runs of the null model (see Section 2.6.1). Since the null distributions for the different behavioral conditions were indistinguishable, we only reported one for brevity. (**GSCC**: Giant Strongly Connected Component; **NM**: Null Model).

That is, there are just a few links that deviate from the main common structure. In other words, most high-weight links are used for direct communication between hubs and the rest of the network, lowering the level of complexity compared to Stop trials. Conversely, during Stop trials, a complicated rearrangement

happens, with denser communications and high-content information traveling more within the large component than outwards. Furthermore, the proximity of the Stop trial curves to the null model (NM) curve reveals that, while they differ from a purely random situation, they share some of its communication rules. Indeed, in the null model, which is complex by definition, one would expect a configuration in which the links are randomly arranged regardless of their weights, resulting in a network dense with paths between nodes but with no stable configurations (as evidenced by the gray curve's sudden descent without intermediate steps) and, most importantly, no hubs (see also Supplementary Figure S5). The slope of the curves in panel c demonstrates that the quantity of information necessary to obtain equivalent stable configurations (i.e., the same values of y in panel a) is smaller in Go trials than in Stop trials. This suggests that the latter's higher inherent complexity relates to increased resource recruitment. These quantitative findings confirm, on a global scale, the intuitions of Figure 4, revealing how the local connections of the clusters change the overall state of the network, modifying its organization and shaping the pattern of information transmission. Furthermore, using TE as a measure for link weights reinforces the conclusions reached in our previous work about the topological state that characterizes planned movement generation and inhibition[24].

### 3.4 Distinctive interactions among neuronal clusters characterize behavioral conditions

Figure 7 depicts the average strength of interaction among network modules (group of nodes) aggregated by cluster during successful Stop trials and Go trials in PMd. The size of the arrows represents the value of **I**, which is the weighted total of TE for all nodes in the same cluster (see also Tables S3 and S4). Following this diagram, the **C_3** cluster is the primary determinant of the global network state, while the **C_1** and **C_2** play supporting roles that are dependent on the behavioral outcome. The **C_1** and **C_2**, respectively, distribute the second-highest information content in Go trials and correct Stop trials (wrong Stop trials are not displayed; see Tables S3 and S4). When movements were generated (in Go trials and wrong Stop trials), the link from the **C_1** to the **C_4** had the greatest **I** value, except from the one from the **C_3**. In contrast, the **C_1** ' contributions to the **C_2** and **C_3** were negligible. In trials with successful inhibition, the highest value of **I** was detected from the **C_2** to the **C_4**, in addition to the one from the **C_3**. Furthermore, the strength and direction of the interactions between the **C_1** and **C_2** hint at the specialization of these clusters during diverse behavioral conditions. In particular, information passed from the **C_2** to the **C_1** in correct Stop trials. Conversely, in Go trials, information traveled from the **C_1** to the **C_2**. The flow of information from the **C_1** and **C_2** to the **C_3** followed the same pattern. The network topology during wrong Stop trials was, as expected, a hybrid of the configurations observed in Go and correct Stop trials.

### 3.5 A recap

In summary, we proved the existence of diverse neural modules/clusters (Figure 4) and we described how these clusters distribute information diversely (Table S2), contributing to the overall state of the mesoscopic network and its level of complexity, each with its own distinct features (Figures 5 and 6). All this defines a hierarchy (or role) within the analyzed PMd network. We refined the hierarchy even further by analyzing how each cluster communicated with the others under the behavioral conditions of the task, demonstrating differences in information processing between correct Stop, Go and wrong Stop trials. Furthermore, we discovered that correct and wrong Stop trials have the same overall topological organization but differ in the details of information processing. Wrong Stop trials revealed a mix of interactions between clusters comparable to those observed in Go trials as well as evidence of attempted inhibition. Finally, our findings revealed a well-defined hierarchical scheme, in which **C_3** are the pivotal nodes in the network, with the **C_1** and **C_2** providing critical support in movement generation and

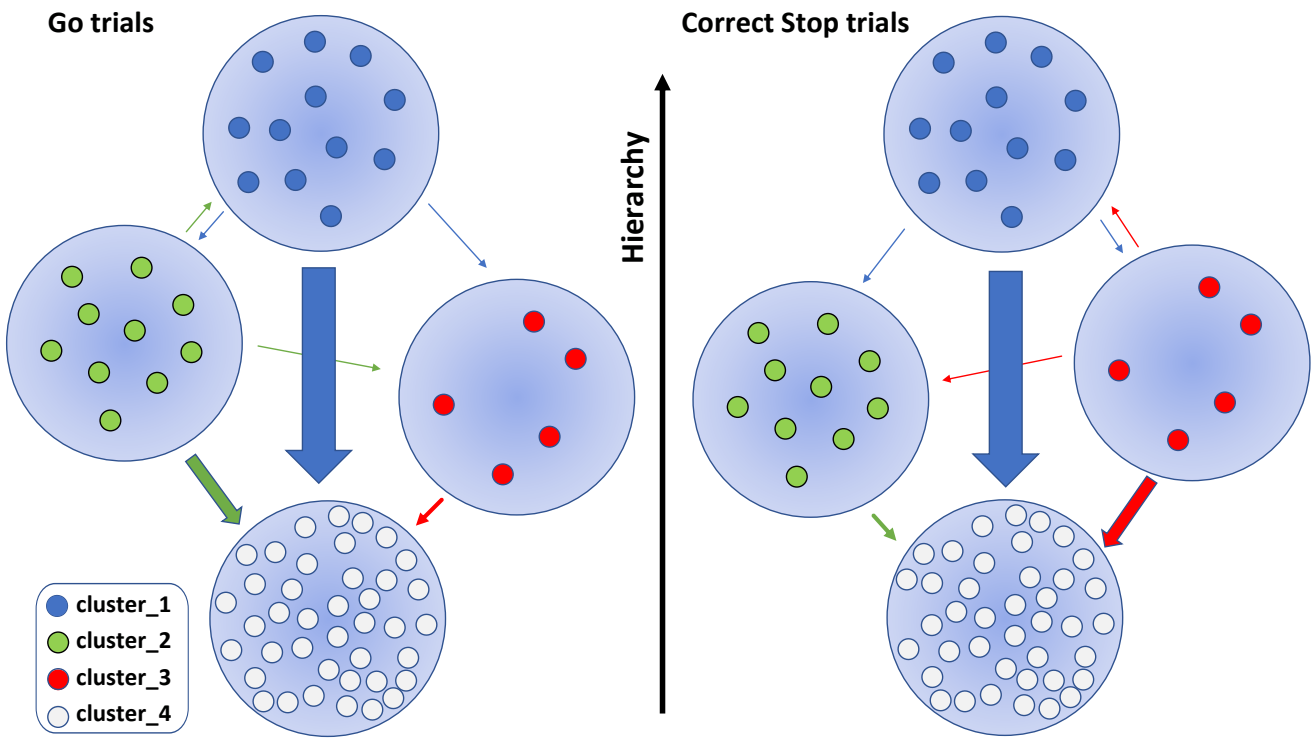


**Figure 7. Information spreading among clusters before movement generation and cancellation**. Arrows between groups of modules are scaled according to the corresponding average value of **I** (among sessions and animals). The level of hierarchy in which each cluster is ranked is graphically represented as the vertical positioning of the nodes; such level depends on the set of measures explored and could be efficiently summarized by the index I. Since the **C_3** is the dominant cluster in the network, its interactions are always shown. For the other clusters, only the interactions at least one order of magnitude greater than the others and statistically significant across behavioral conditions are shown (see Tables S3 and S4 for further details).

inhibition, respectively.

# 4 Discussion

In this work, we investigated the patterns of local information transfer in a cortical network directly involved in movement decision-making (the PMd). We used a combined TE and graph theory-based approach to analyze the aggregate spiking activity of simultaneously recorded populations of neurons. Our results contribute to moving forward the knowledge on the neural basis of motor control at different levels.

## 4.1 A topological approach to local information propagation in a motor decision task

The first level of advancement is methodological. Although TE is growing in popularity in modern neuroscience, its application to invasive electrophysiological data to study patterns of directed connectivity has been so far very limited and restricted mostly to either single neurons[51,80] or in vitro[51,81–84] and in silico studies[39]. Shimono and Beggs and Nigam et al., used it at the single neuron level to investigate the structure at different scales of the rodent somatosensory cortex[51,85]. Thivierge[83] used TE to examine the statistical dependencies between spontaneous neural activity recorded in cultures of cortical neurons. Timme and colleagues[86] recorded the activity of hundreds of neurons in cortico-hippocampal slice cultures

and used TE to study the information transfer changes therein. An early contribution to this research topic is from Gerhard et al[87] that inspected the topology of spike trains recordings from the visual system of a rhesus monkey during a fixation task. However, the authors employed a different approach to measure directed connectivity (the use of TE on invasive electrophysiological data from the visual system is also attributable to Besserve and colleagues[88] which however did not resort to graph theory techniques). Another contribution comes from the work of Honey and colleagues, who explored the relationship between the functional and structural properties of a large-scale interregional anatomical network of the macaque cortex through TE[89]. Here, both the spatial and the temporal scale of analysis were completely different: the authors simulated the time series of each brain region through nonlinear models of spontaneous neuronal activity. Wollstadt and collaborators also considered larger spatial and temporal scales than the one here presented[37]. Their work is of particular significance because it introduces for the first time a powerful method to estimate TE under nonstationary conditions, the so-called ensemble method. Such method exploits the multi-trial structure in neuroscience data to pool observation of neural activity over the ensemble of repeated trials instead of time, leading to a very accurate time-resolved TE. This represents a difference from the present work, where, instead, the exchange of information within the system is inferred in a fixed time window. Our choice was motivated by our interest to characterize the state of the PMd information network at a specific epoch of the task and compare it across behavioral conditions. To do so, we needed several network realizations (over trials) in order to obtain a statistically robust estimate of its topological properties. In contrast, the ensemble approach would have led to a single representation of the temporal evolution of the network. A temporally precise but unique one. It could be argued that this constitutes a limitation of our analysis. Instead, we believe it is the way to answer a different scientific question. We also believe that the ensemble method is extremely powerful and it could be of interest to use it on our data in future studies. An attempt to study voluntary action control through analysis of directed connectivity was made by Jahfari and colleagues[90] but on human MRI data. Hence, to the best of our knowledge, this report is one of two studies that use graph theory to analyze the information transfer network of a specific cortical area at the mesoscale level *in vivo* and during a behavioral task. The only other work on the topic known to us is the extremely recent paper from Varley et al.[80] who, using the same dataset as Dann et al.[91], quantified information transmission between single neurons in the fronto-parietal areas AIP, F5, and M1 during various epochs of a delayed grasping task. The authors compared several components of information processing, including also a multi-variate estimate of Transfer Entropy very similar to ours, and inspected how they changed as the task unfolded (see next paragraph). The level of description here obtained is more detailed compared to previous works on motor control. Indeed, we were able to specify how the decision on whether to move or to stop is implemented in PMd at the meso-scale population level, who are the (key) players that manage information transmission, and how information propagation shape the hierarchies and the complexity of the network depending on the behavioral conditions. Notably, in our framework, neither any a priori assumption nor a specific neural modeling technique was needed. Our completely data-driven approach, in addition to complement the most recent models for the motor generation and suppression[92,93], permits us to overcome their main limitation which resides in the requirement of many biophysical parameters to be tweaked and tuned before fitting with acceptable accuracy the experimental data. In this regard, recently, more and more authors are applying graph theory tools to the study of neuronal interactions in different contexts and at diverse spatial scales. This provides great advantages in the case of inferential models that aim to estimate complex networks that represent functional and/or anatomical interactions between single neurons or entire brain areas[94,95]. It also proves particularly useful when one wants to directly analyze experimental brain networks and reconstruct their generative models[44,96,97]. For all these reasons, although is still not largely used in behavioral neurophysiological studies at the small and mesoscale, a

graph theory-based conceptualization of neural interactions, possibly united with information theoretic measures, can be very profitable also compared to other common approaches relying on the analysis of covariance between neurons or mesoscopic signals[14,22,98–101] and should be exploited more. In fact, these methods are not straightforward in distinguishing the specific contributions of single neurons (or discrete populations of neurons) to the topology of network dynamics, which is our strategy's strength. On one hand, this range of methods allows for a fine temporal description of neural variability but on the other, due to their nature, are neither capable to describe the information flow between neuronal actors nor to provide quantitative insights on the topology of network connections and their hierarchical organization. Without this spectrum of details the computational strategy underlying motor control (and neural circuitry computation in general) would be yet elusive. In recent times, some other authors have started to follow the joint information theory-complex networks approach but for now, to the best of our knowledge, only on cortico-hippocampal[86], somatosensory cortex slice cultures[45,51,84] and during anesthesia[102]. It is known that to fully understand the neural mechanisms behind motor control future research should focus on cortico-cortical and cortico-subcortical interactions through massive simultaneous recordings. In this scenario, a topological information-based approach would be unquestionably necessary to gain an overall view and elicit detailed insights.

### 4.2 Fine-grained information transfer underlies motor decisions in PMd

The second level of advancement, which is closely related to the first, concerns the novelty of our results compared to other studies, especially those that focused on the interaction among clusters of neuronal assemblies during motor decision. We found, in the characterized PMd network, that neuronal activities could be organized in four clusters that actively participate, with distinct roles, i.e., through different topological attributes, both in movement execution and cancellation. This is a step forward in the conceptualization of the neural processes that underlie movement generation. Indeed, other studies describe movement generation as the result of accumulation processes toward a threshold, or as a transition of neuronal trajectories across specific subspaces. Some studies describe the accumulation process as instantiated by specific neuronal types (as for gaze-shifting neurons in the frontal eye field and in the superior colliculus for saccades): others consider the neuronal trajectory reflecting the dynamics of the entire neuronal population without considering specific neuronal types. units[21,22,92,93,103–106] We showed that information is hierarchically transferred between more actors, with a cluster (C_3) acting as the most important hub for information spreading across behavioral conditions. This reflects the existence of an intrinsic high-order complexity in functional communications at the population level, even in small portions of the cortex, during behavioral control, regardless of which the nature of neurons in each cluster might be (e.g., excitatory or inhibitory neurons). Based only on the information exchanged by each local module, we managed to isolate both condition-specific and nonspecific neuronal clusters. It is worth stressing that we drew our conclusion in a completely data-driven and model-free fashion, and this strengthens the results.

Additionally, we showed to what extent the information transfer and the level of complexity within the network are dependent on the behavioral outcomes. Our picture integrates the current view because besides specific clusters more involved in the generation (C_1 cluster) or inhibition (C_2 cluster) of movements, it establishes the existence of a high order cluster (C_3 cluster) not proposed in other works, portraying the interaction patterns beneath inhibitory control at the PMd level (see Fig. 7). Topologically speaking, the extent of theorization about neural processes underlying motor control is pushed further by the degree of formalization that percolation analysis allows. Regarding the behavioral functionality, according to the race model, the Stop process should be 'activated' only in the Stop trials following the presentation of the Stop signal. However, increasing evidence[107,108] suggests that the Stop process is also active in Go trials.

Our results show that at the level of information propagation in the PMd, such co-activation corresponds to information revolving around four clusters arranged in higher-order connectivity patterns. This is matched by the hierarchical levels in which the C_1 cluster and C_2 cluster are ranked in the different behavioral conditions. Moreover, our results also show that the C_2 cluster exhibits a flow of information directed to the C_3 cluster that is significantly higher during correct Stop trials compared to the other behavioral conditions. This suggests that some of the information that the C_2 cluster handles in attempting to abort the movement is directed to influence the C_3 cluster, which are extensively involved in facilitating the overall process. This evidence suggests that the reason why the attempt fails in the wrong Stop trials is related to the strong flow directed from the C_1 cluster to the C_4 cluster, as it occurs in the Go trials and to the limited involvement of the C_2 cluster, which distribute considerably less information than in the case of properly inhibited movements (see also Table S3). This highlights, for the first time at the mesoscale resolution, the existence of a fine-grained organization of neural assemblies at the population level that handle intra-area information flow. It is worth pointing out that "usual" methods of studying neural activity profiles are not sufficient to infer all aspects of such architecture. The found subdivision in clusters, the presence of hubs, i.e. topological central nodes deputed to sort out the communications, reveal that the cortical information dynamics behind motor control is extremely rich and must be accounted for to generate more comprehensive models. The topological organization we portrayed also implies that the presence of high-degree nodes is a constituent feature of neural processing in a cortical network directly involved in cognitive control, as is the PMd. This is reinforced by the finding that the topological structure detected across behavioral conditions exhibits stable rules for the information transmission system: the one based on hubs. This is consistent with our previous study[24], in which we showed how the functional PMd network organization differs between movement generation and inhibition in terms of hierarchy and centrality of nodes. It is also in agreement with other works that found high degree nodes in silico[109], in cortical and hippocampal in vitro networks[51,53,85,86,110–112], in vivo[80,91] and anatomical structural networks[89]. Within this topology, different information exchange regimes are realized, which are reflected in specific quantifiable differences. On one hand, correct and wrong Stop trials resulted in similar levels of complexity. On the other, during Go and wrong Stop trials clusters were recruited to exchange information in a similar fashion. This attests that the peculiarities of the information network depend on the outcome of the motor behavior, passing from a purely centralized state during Go trials to a dissimilar one during Stop trials, the latter characterized by a higher level of complexity, an increased degree of randomness and a distinctive scheme of information transfer. This change is of particular interest because it signals a strong association between the mode of communication between nodes and the specific behavioral condition. Most notably, the structure found in the Go trials implies a high and very robust communication strategy compared to that observed in trials in which a Stop is presented. Considering also the results from our previous study[24], this appears to be the preferred mode of information transmission, at the PMd level, when a movement is planned and then executed. Similarly, the network state to be associated with a planned and then inhibited movement seems to correspond to one that is topologically very similar to the previous one but in which some degree of randomness is, however, "injected" into the interactions. What demonstrated in the present work adds a very important piece to the puzzle, that of the fine-grained, yet flexible, hierarchical organization realized through the clusters. All this gives us an insight into how a network involved in a cognitive task is capable of changing the goal of its functionality by changing its degree of complexity and heterogeneity, recruiting varying resources but keeping the generating rules of its topology stable. In particular, we interpret the reorganization occurring in correct Stop trials as the execution in the local network, through the intervention of the C_2 cluster, of a command originating from other regions. Indeed, as known, the PMd is part of a larger network subserving motor control based on frontal, parietal, subcortical and spinal structures. It is reasonable to think that during Go trials the hubs

serve to convey the command to move to other (and possibly anatomically lower) cortical, subcortical, and spinal circuits that will eventually promote muscle activation. In this picture, the state observed during correct Stop trials could reflect the PMd collective reaction to the incoming inhibitory input that prevents the execution of the programmed movement. Therefore, the volition to inhibit would be locally implemented as 'the attenuation of the movement state', that would be obtained by tuning the level of randomness in the wiring scheme of the network with a resulting more complex organization. This seems convenient and easy to implement at the level of network dynamics in that it would be sufficient, in order to spread the message, to recruit dedicated resources (the C_2 cluster) and to detour the information flow through different paths between nodes. Along these lines, the state recorded during a wrong Stop, being topologically relatable to that of a correct Stop and, at the same time, showing the same patterns of information transfer of Go trials, would result from an erroneous transmission of the inhibitory coding. Probably due to a persistent strong recruitment of the C_1 cluster and a contemporary weaker involvement of the C_2 cluster, as it happens during Go trials. This is in agreement with what we described in one of our recent papers in which we analyzed the dynamics of neural activity in the same task with a state-space approach[22]. Indeed, in that scenario, we demonstrated how a subspace in which neural activities are confined before movement generation and during movement suppression exists.

One weakness of this study is that we cannot account for the information dynamics between PMd and other structures of the reaching network. Therefore, additional research, in a multi-area framework, will be needed to unambiguously clarify the interactions of the PMd network with other structures and to investigate to whom the clusters project or are connected to. The multi-area approach is instead a strength of Varley's and colleagues work[80] with which our results are only partially comparable, as they did not record from the PMd and the task they analyzed did not include inhibition trials. For the shared part (the movement trials), the results are in agreement: the presence of hierarchical hubs also emerged as a core topological attribute in their case, further confirming the ubiquitous presence of this feature of neural organization in cognitive control. Moreover, the 'processing units' they described, emerge from averaged interactions of macro ensembles of neurons, thus neglecting their decomposition into individual contributions (and their interactions) within the same area. Both works thus have their strengths and weaknesses, testifying how for a more complete understanding this type of approach needs to be systematized. Considering the nature of the mesoscopic signal we studied, it was not possible to resolve the contributions of individual neurons within each of the modules forming the clusters. This is related to another question that remains unexplored in this article: whether and how the excitatory/inhibitory nature of individual neurons could affect cluster composition and role. To this end, the framework of information theory is essential, as extensions of the TE measure have recently been proposed to track the excitatory or inhibitory signatures of information exchange between neurons[44,84]. Our findings clearly show that hierarchical control is not only exerted across brain regions , but it is also implemented locally by specific neuronal clusters (the C_3 cluster in our case) over the others. This is in line with evidence provided in recent years that the brain is hierarchically organized both globally and locally on a spatial[24,60,80,113–123] (for a detailed review see Hilgetag et al., 2020[124]) and temporal scale[125–131]. As far as we know, this is the first work that deeply investigates the local information topology of a single cortical area known to have a crucial role in the motor system. These conclusions suggest that the collective network organization we discovered represents the neural implementation for the voluntary motor control at the PMd level.

## Acknowledgements

Partially supported by grants from Sapienza University (PH11715C823A9528 to SF and RM11916B89232364 to PP), from EC FP7 grant 'BrainLeap' (to SF), from grant 'Borse di Studio 2020' Fondazione Baroni (to GB), and from EC ERANET CHIST-ERA 2019 grant 'MUCCA' (to SF).

## Author contributions statement

F.G, P.P., E.B. and S.F conceived the experiment, F.G. and P.P. conducted the experiment, G.B. analysed the results. All authors contributed to critical discussion and reviewed the manuscript.

## Data availability statement

Data are available from the corresponding author upon reasonable request.

## Competing interests

The authors report no declarations of interest.

## References


1. Georgopoulos, A. P., Kalaska, J. F., Caminiti, R. & Massey, J. T. On the relations between the direction of two-dimensional arm movements and cell discharge in primate motor cortex. *The J. neuroscience : official journal Soc. for Neurosci.* **2**, 1527–1537, 10.1523/JNEUROSCI.02-11-01527.1982 (1982).

2. Caminiti, R., Johnson, P. B., Galli, C., Ferraina, S. & Burnod, Y. Making arm movements within different parts of space: the premotor and motor cortical representation of a coordinate system for reaching to visual targets. *J. Neurosci.* **11**, 1182–1197, 10.1523/JNEUROSCI.11-05-01182.1991 (1991).

3. Riehle, A., Grün, S., Diesmann, M. & Aertsen, A. Spike synchronization and rate modulation differentially involved in motor cortical function. *Science* **278**, 1950–1953, 10.1126/science.278.5345.1950 (1997).

4. Munoz, D. P. & Wurtz, R. H. Fixation cells in monkey superior colliculus I. Characteristics of cell discharge. *J. Neurophysiol.* **70**, 559–575, 10.1152/jn.1993.70.2.559 (1993).

5. Vaadia, E., Kurata, K. & Wise, S. P. Neuronal activity preceding directional and nondirectional cues in the premotor cortex of rhesus monkeys. *Somatosens. & Mot. Res.* **6**, 207–230, 10.3109/08990228809144674 (1988).

6. Fetz, E. E. Are movement parameters recognizably coded in the activity of single neurons? *Behav. Brain Sci.* **15**, 679–690, 10.1017/S0140525X00072599 (1992).

7. Ferraina, S., Paré, M. & Wurtz, R. H. Comparison of cortico-cortical and cortico-collicular signals for the generation of saccadic eye movements. *J. Neurophysiol.* **87**, 845–858, 10.1152/jn.00317.2001 (2002).

8. Wurtz, R. H., Sommer, M. A., Paré, M. & Ferraina, S. Signal transformations from cerebral cortex to superior colliculus for the generation of saccades. *Vis. Res.* **41**, 3399–3412, 10.1016/S0042-6989(01)00066-9 (2001).

9. Hong, G. & Lieber, C. M. Novel electrode technologies for neural recordings. *Nat. Rev. Neurosci.* **20**, 330–345, 10.1038/s41583-019-0140-6 (2019).

10. Shenoy, K. V., Sahani, M. & Churchland, M. M. Cortical Control of Arm Movements: A Dynamical Systems Perspective. *Annu. Rev. Neurosci.* **36**, 337–359, 10.1146/annurev-neuro-062111-150509 (2013).

11. Herreras, O. Local Field Potentials: Myths and Misunderstandings. *Front. Neural Circuits* **10**, 101, 10.3389/fncir.2016.00101 (2016).

12. Stark, E. & Abeles, M. Predicting movement from multiunit activity. *J. Neurosci.* **27**, 8387–8394, 10.1523/JNEUROSCI.1321-07.2007 (2007).

13. Trautmann, E. M. *et al.* Accurate Estimation of Neural Population Dynamics without Spike Sorting. *Neuron* **103**, 292–308, 10.1016/j.neuron.2019.05.003 (2019).

14. Mattia, M. *et al.* Heterogeneous attractor cell assemblies for motor planning in premotor cortex. *J. Neurosci.* **33**, 11155–11168, 10.1523/JNEUROSCI.4664-12.2013 (2013).

15. Supèr, H. & Roelfsema, P. R. Chronic multiunit recordings in behaving animals: advantages and limitations. *Prog. Brain Res.* **147**, 263–282, 10.1016/S0079-6123(04)47020-4 (2005).

**16.** Wise, S. P., Boussaoud, D., Johnson, P. B. & Caminiti, R. Premotor and parietal cortex: Corticocortical connectivity and combinatorial computations. *Annu. Rev. Neurosci.* **20**, 25–42, 10.1146/annurev.neuro.20.1.25 (1997).

**17.** Cisek, P. & Kalaska, J. F. Neural mechanisms for interacting with a world full of action choices. *Annu. Rev. Neurosci.* **33**, 269–298, 10.1146/annurev.neuro.051508.135409 (2010).

**18.** Milekovic, T., Truccolo, W., Grün, S., Riehle, A. & Brochier, T. Local field potentials in primate motor cortex encode grasp kinetic parameters. *NeuroImage* **114**, 338–355, 10.1016/J.NEUROIMAGE.2015.04.008 (2015).

**19.** Logan, G. D. & Cowan, W. B. On the ability to inhibit thought and action: A theory of an act of control. *Psychol. Rev.* **91**, 295–327, 10.1037//0033-295x.91.3.295 (1984).

**20.** Mirabella, G., Pani, P. & Ferraina, S. Neural correlates of cognitive control of reaching movements in the dorsal premotor cortex of rhesus monkeys. *J. Neurophysiol.* **106**, 1454–1466, 10.1152/jn.00995.2010 (2011).

**21.** Marcos, E. *et al.* Neural variability in premotor cortex is modulated by trial history and predicts behavioral performance. *Neuron* **78**, 249–255, 10.1016/j.neuron.2013.02.006 (2013).

**22.** Pani, P. *et al.* Neuronal population dynamics during motor plan cancellation in nonhuman primates. *Proc. Natl. Acad. Sci. United States Am.* **119**, e2122395119, 10.1073/pnas.2122395119 (2022).

**23.** Pani, P. *et al.* Alpha- and beta-band oscillations subserve different processes in reactive control of limb movements. *Front. behavioral neuroscience* **8**, 10.3389/FNBEH.2014.00383 (2014).

**24.** Bardella, G., Pani, P., Brunamonti, E., Giarrocco, F. & Ferraina, S. The small scale functional topology of movement control: Hierarchical organization of local activity anticipates movement generation in the premotor cortex of primates. *NeuroImage* **207**, 10.1016/j.neuroimage.2019.116354 (2020).

**25.** Hanes, D. P., Patterson, W. F. & Schall, J. D. Role of frontal eye fields in countermanding saccades: Visual, movement, and fixation activity. *J. Neurophysiol.* **79**, 817–834, 10.1152/jn.1998.79.2.817 (1998).

**26.** Paré, M. & Hanes, D. P. Controlled movement processing: Superior colliculus activity associated with countermanded saccades. *J. Neurosci.* **23**, 6480–6489, 10.1523/jneurosci.23-16-06480.2003 (2003).

**27.** Bassett, D. S. & Sporns, O. Network neuroscience. *Nat. Neurosci. 2017 20:3* **20**, 353–364, 10.1038/nn.4502 (2017).

**28.** Band, G. P., van der Molen, M. W. & Logan, G. D. Horse-race model simulations of the stop-signal procedure. *Acta Psychol.* **112**, 105–142, 10.1016/S0001-6918(02)00079-3 (2003).

**29.** Mattia, M. & Del Giudice, P. Population dynamics of interacting spiking neurons. *Phys. Rev. E - Stat. Physics, Plasmas, Fluids, Relat. Interdiscip. Top.* **66**, 19, 10.1103/PhysRevE.66.051917 (2002).

**30.** Choi, Y. S., Koenig, M. A., Jia, X. & Thakor, N. V. Quantifying time-varying multiunit neural activity using entropy-based measures. *IEEE Transactions on Biomed. Eng.* **57**, 2771–2777, 10.1109/TBME.2010.2049266 (2010).

**31.** Sharma, G. *et al.* Time Stability and Coherence Analysis of Multiunit, Single-Unit and Local Field Potential Neuronal Signals in Chronically Implanted Brain Electrodes. *Bioelectron. Medicine 2015 2:1* **2**, 63–71, 10.15424/BIOELECTRONMED.2015.00010 (2015).

**32.** Schreiber, T. Measuring information transfer. *Phys. Rev. Lett.* **85**, 461–464, 10.1103/PhysRevLett.85.461 (2000).

**33.** Komárek, V., Hrnčíř, Z. & Štěrbová, K. Synchronization as adjustment of information rates: Detection from bivariate time series. *Phys. Rev. E* **63**, 046211, 10.1103/PhysRevE.63.046211 (2001).

**34.** Ursino, M., Ricci, G. & Magosso, E. Transfer Entropy as a Measure of Brain Connectivity: A Critical Analysis With the Help of Neural Mass Models. *Front. Comput. Neurosci.* **14**, 534148, 10.3389/FNCOM.2020.00045/BIBTEX (2020).

**35.** Novelli, L. & Lizier, J. T. Inferring network properties from time series using transfer entropy and mutual information: Validation of multivariate versus bivariate approaches. *Netw. Neurosci.* **5**, 373–404, 10.1162/NETN{_}A{_}00178 (2021).

**36.** Xiong, W., Faes, L. & Ivanov, P. C. Entropy measures, entropy estimators, and their performance in quantifying complex dynamics: Effects of artifacts, nonstationarity, and long-range correlations. *Phys. Rev. E* **95**, 1–37, 10.1103/PhysRevE.95.062114 (2017).

**37.** Wollstadt, P., Martínez-Zarzuela, M., Vicente, R., Díaz-Pernas, F. J. & Wibral, M. Efficient transfer entropy analysis of non-stationary neural time series. *PLoS ONE* **9**, 102833, 10.1371/journal.pone.0102833 (2014).

**38.** Vicente, R., Wibral, M., Lindner, M. & Pipa, G. Transfer entropy-a model-free measure of effective connectivity for the neurosciences. *J. Comput. Neurosci.* **30**, 45–67, 10.1007/s10827-010-0262-3 (2011).

**39.** Ito, S. *et al.* Extending Transfer Entropy Improves Identification of Effective Connectivity in a Spiking Cortical Network Model. *PLoS ONE* **6**, e27431, 10.1371/journal.pone.0027431 (2011).

**40.** Wibral, M. *et al.* Transfer entropy in magnetoencephalographic data: Quantifying information flow in cortical and cerebellar networks. *Prog. Biophys. Mol. Biol.* **105**, 80–97, 10.1016/j.pbiomolbio.2010.11.006 (2011).

**41.** Michael Wibral, J. T. L., Raul Vicente (ed.) *Directed Information Measures in Neuroscience | SpringerLink* (Springer Berlin, Heidelberg, 2014), 1 edn.

**42.** Ramos, A. M. T., Macau, E. E. N., Lopes, A. M. & Machado, J. A. T. Minimum Sample Size for Reliable Causal Inference Using Transfer Entropy. *Entropy 2017* **19**, 150, 10.3390/E19040150 (2017).

**43.** Bossomaier, T., Barnett, L., Harré, M. & Lizier, J. T. *An introduction to transfer entropy: Information flow in complex systems* (Springer International Publishing, 2016).

**44.** Goetze, F. & Lai, P. Y. Reconstructing positive and negative couplings in Ising spin networks by sorted local transfer entropy. *Phys. Rev. E* **100**, 012121, 10.1103/PHYSREVE.100.012121/FIGURES/6/MEDIUM (2019).

**45.** Newman, E. L., Varley, T. F., Parakkattu, V. K., Sherrill, S. P. & Beggs, J. M. Revealing the Dynamics of Neural Information Processing with Multivariate Information Decomposition. *Entropy 2022, Vol. 24, Page 930* **24**, 930, 10.3390/E24070930 (2022).

**46.** Montalto, A., Faes, L. & Marinazzo, D. MuTE: A MATLAB toolbox to compare established and novel estimators of the multivariate transfer entropy. *PLoS ONE* **9**, e109462, 10.1371/journal.pone.0109462 (2014).

**47.** Faes, L., Kugiumtzis, D., Nollo, G., Jurysta, F. & Marinazzo, D. Estimating the decomposition of predictive information in multivariate systems. *PHYSICAL REVIEW E* **91**, 32904, 10.1103/PhysRevE.91.032904 (2015).

**48.** Shannon, C. E. A Mathematical Theory of Communication. *The Bell Syst. Tech. J.* **27**, 623–656 (1948).

**49.** Faes, L., Marinazzo, D., Montalto, A. & Nollo, G. Lag-specific transfer entropy as a tool to assess cardiovascular and cardiorespiratory information transfer. *IEEE Transactions on Biomed. Eng.* **61**, 2556–2568, 10.1109/TBME.2014.2323131 (2014).

**50.** Faes, L., Nollo, G. & Porta, A. Information-based detection of nonlinear Granger causality in multivariate processes via a nonuniform embedding technique. *Phys. Rev. E - Stat. Nonlinear, Soft Matter Phys.* **83**, 051112, 10.1103/PhysRevE.83.051112 (2011).

**51.** Shimono, M. & Beggs, J. M. Functional clusters, hubs, and communities in the cortical microconnectome. *Cereb. Cortex* **25**, 3743–3757, 10.1093/cercor/bhu252 (2015).

**52.** Timme, N. M. *et al.* High-Degree Neurons Feed Cortical Computations. *PLOS Comput. Biol.* **12**, e1004858, 10.1371/journal.pcbi.1004858 (2016).

**53.** Antonello, P. C. *et al.* Self-organization of in vitro neuronal assemblies drives to complex network topology. *eLife* **11**, 10.7554/ELIFE.74921 (2022).

**54.** Mason, A., Nicoli, A. & Stratford, K. Synaptic transmission between individual pyramidal neurons of the rat visual cortex in vitro. *J. Neurosci.* **11**, 72–84, 10.1523/JNEUROSCI.11-01-00072.1991 (1991).

**55.** Swadlow, H. A. Efferent neurons and suspected interneurons in motor cortex of the awake rabbit: axonal properties, sensory receptive fields, and subthreshold synaptic inputs. *J. neurophysiology* **71**, 437–453, 10.1152/JN.1994.71.2.437 (1994).

**56.** Barthó, P. *et al.* Characterization of neocortical principal cells and interneurons by network interactions and extracellular features. *J. neurophysiology* **92**, 600–608, 10.1152/JN.01170.2003 (2004).

**57.** Gómez-Herrero, G. *et al.* Assessing Coupling Dynamics from an Ensemble of Time Series. *Entropy 2015, Vol. 17, Pages 1958-1970* **17**, 1958–1970, 10.3390/E17041958 (2015).

**58.** Timme, N. M. & Lapish, C. A Tutorial for Information Theory in Neuroscience. *eNeuro* **5**, 10.1523/ENEURO.0052-18.2018 (2018).

**59.** Callaway, D. S., Newman, M. E., Strogatz, S. H. & Watts, D. J. Network Robustness and Fragility: Percolation on Random Graphs. *Phys. Rev. Lett.* **85**, 5468, 10.1103/PhysRevLett.85.5468 (2000).

**60.** Bardella, G., Bifone, A., Gabrielli, A., Gozzi, A. & Squartini, T. Hierarchical organization of functional connectivity in the mouse brain: A complex network approach. *Sci. Reports* **6**, 1–11, 10.1038/srep32060 (2016).

**61.** Gallos, L. K., Makse, H. A. & Sigman, M. A small world of weak ties provides optimal global integration of self-similar modules in functional brain networks. *Proc. Natl. Acad. Sci. United States Am.* **109**, 2825–2830, 10.1073/pnas.1106612109 (2012).

**62.** Nicolini, C., Bordier, C. & Bifone, A. Community detection in weighted brain connectivity networks beyond the resolution limit. *NeuroImage* **146**, 28–39, 10.1016/j.neuroimage.2016.11.026 (2017).

**63.** Nicolini, C. & Bifone, A. Modular structure of brain functional networks: breaking the resolution limit by Surprise. *Sci. Reports* **6**, 10.1038/SREP19250 (2016).

**64.** Vlasov, V. & Bifone, A. Hub-driven remote synchronization in brain networks. *Sci. Reports 2017 7:1* **7**, 1–11, 10.1038/s41598-017-09887-7 (2017).

**65.** Mastrandrea, R. *et al.* Organization and hierarchy of the human functional brain network lead to a chain-like core. *Sci. Reports 2017 7:1* **7**, 1–13, 10.1038/s41598-017-04716-3 (2017).

**66.** Mastrandrea, R. *et al.* The unbalanced reorganization of weaker functional connections induces the altered brain network topology in schizophrenia. *Sci. Reports* **11**, 15400, 10.1038/S41598-021-94825-X (2021).

**67.** Bordier, C., Nicolini, C. & Bifone, A. Graph analysis and modularity of brain functional connectivity networks: Searching for the optimal threshold. *Front. Neurosci.* **11**, 441, 10.3389/fnins.2017.00441 (2017).

**68.** Bordier, C., Nicolini, C., Forcellini, G. & Bifone, A. Disrupted modular organization of primary sensory brain areas in schizophrenia. *NeuroImage: Clin.* **18**, 682–693, 10.1016/j.nicl.2018.02.035 (2018).

**69.** Del Ferraro, G. *et al.* Finding influential nodes for integration in brain networks using optimal percolation theory. *Nat. Commun. 2018 9:1* **9**, 1–12, 10.1038/s41467-018-04718-3 (2018).

**70.** Graf, A. On the Strongly Connected Components of Random Directed Graphs with Given Degree Sequences. Tech. Rep., University of Waterloo (2016).

**71.** Squires, S. *et al.* Weakly explosive percolation in directed networks. *PHYSICAL REVIEW E* **87**, 52127, 10.1103/PhysRevE.87.052127 (2013).

**72.** Albert, R. & Barabási, A.-L. Statistical mechanics of complex networks. *Rev. Mod. Phys.* **74**, 47–97, 10.1103/RevModPhys.74.47 (2002).

**73.** Barabási, A. L. Network science, 10.1098/rsta.2012.0375 (2013).

**74.** Barabási, A. L. & Albert, R. Emergence of scaling in random networks. *Science* **286**, 509–512, 10.1126/science.286.5439.509 (1999).

**75.** Cimini, G. *et al.* The statistical physics of real-world networks. *Nat. Rev. Phys.* **1**, 58–71, 10.1038/s42254-018-0002-6 (2019).

**76.** Ramawat, S. *et al.* Different Contribution of the Monkey Prefrontal and Premotor Dorsal Cortex in Decision Making During a Transitive Inference Task. *Neuroscience* **485**, 147–162, 10.1016/J.NEUROSCIENCE.2022.01.013 (2022).

**77.** Pani, P. *et al.* Visual salience of the stop signal affects the neuronal dynamics of controlled inhibition. *Sci. Reports 2018 8:1* **8**, 1–13, 10.1038/s41598-018-32669-8 (2018).

**78.** Battaglia-Mayer, A. *et al.* Correction and suppression of reaching movements in the cerebral cortex: Physiological and neuropsychological aspects, 10.1016/j.neubiorev.2014.03.002 (2014).

**79.** Giarrocco, F. *et al.* Neuronal dynamics of signal selective motor plan cancellation in the macaque dorsal premotor cortex. *Cortex* **135**, 326–340, 10.1016/j.cortex.2020.09.032 (2021).

**80.** Varley, T. F., Sporns, O., Schaffelhofer, S., Scherberger, H. & Dann, B. Information-processing dynamics in neural networks of macaque cerebral cortex reflect cognitive state and behavior. *Proc. Natl. Acad. Sci. United States Am.* **120**, e2207677120, 10.1073/PNAS.2207677120/SUPPL{_}FILE/PNAS.2207677120.SD05.CSV (2023).

**81.** Buehlmann, A. & Deco, G. Optimal information transfer in the cortex through synchronization. *PLoS Comput. Biol.* **6**, 1000934, 10.1371/journal.pcbi.1000934 (2010).

**82.** Orlandi, J. G., Stetter, O., Soriano, J., Geisel, T. & Battaglia, D. Transfer entropy reconstruction and labeling of neuronal connections from simulated calcium imaging. *PLoS ONE* **9**, 98842, 10.1371/journal.pone.0098842 (2014).

**83.** Thivierge, J.-P. Scale-free and economical features of functional connectivity in neuronal networks. *PHYSICAL REVIEW E* **90**, 22721, 10.1103/PhysRevE.90.022721 (2014).

**84.** Kajiwara, M. *et al.* Inhibitory neurons exhibit high controlling ability in the cortical microconnectome. *PLOS Comput. Biol.* **17**, e1008846, 10.1371/JOURNAL.PCBI.1008846 (2021).

**85.** Nigam, S. *et al.* Rich-club organization in effective connectivity among cortical neurons. *J. Neurosci.* **36**, 655–669, 10.1523/JNEUROSCI.2177-15.2016 (2016).

**86.** Timme, N. *et al.* Multiplex Networks of Cortical and Hippocampal Neurons Revealed at Different Timescales. *PLoS ONE* **9**, e115764, 10.1371/journal.pone.0115764 (2014).

**87.** Gerhard, F., Pipa, G., Lima, B., Neuenschwander, S. & Gerstner, W. Extraction of Network Topology From Multi-Electrode Recordings: Is there a Small-World Effect? *Front. Comput. Neurosci.* **5**, 4, 10.3389/fncom.2011.00004 (2011).

**88.** Besserve, M., Lowe, S. C., Logothetis, N. K., Schölkopf, B. & Panzeri, S. Shifts of Gamma Phase across Primary Visual Cortical Sites Reflect Dynamic Stimulus-Modulated Information Transfer. *PLoS Biol.* **13**, e1002257, 10.1371/journal.pbio.1002257 (2015).

**89.** Honey, C. J., Kötter, R., Breakspear, M. & Sporns, O. Network structure of cerebral cortex shapes functional connectivity on multiple time scales. *Proc. Natl. Acad. Sci. United States Am.* **104**, 10240–10245, 10.1073/pnas.0701519104 (2007).

**90.** Jahfari, S. *et al.* Effective connectivity reveals important roles for both the hyperdirect (fronto-subthalamic) and the indirect (fronto-striatal-pallidal) fronto-basal ganglia pathways during response inhibition. *J. Neurosci.* **31**, 6891–6899, 10.1523/JNEUROSCI.5253-10.2011 (2011).

**91.** Dann, B., Michaels, J. A., Schaffelhofer, S. & Scherberger, H. Uniting functional network topology and oscillations in the fronto-parietal single unit network of behaving primates. *eLife* **5**, 10.7554/eLife.15719 (2016).

**92.** Boucher, L., Palmeri, T. J., Logan, G. D. & Schall, J. D. Inhibitory control in mind and brain: An interactive race model of countermanding saccades. *Psychol. Rev.* **114**, 376–397, 10.1037/0033-295X.114.2.376 (2007).

**93.** Lo, C. C., Boucher, L., Paré, M., Schall, J. D. & Wang, X. J. Proactive inhibitory control and attractor dynamics in countermanding action: A spiking neural circuit model. *J. Neurosci.* **29**, 9059–9071, 10.1523/JNEUROSCI.6164-08.2009 (2009).

**94.** Gupta, G., Pequito, S. & Bogdan, P. Dealing with Unknown Unknowns: Identification and Selection of Minimal Sensing for Fractional Dynamics with Unknown Inputs. *2018 Annu. Am. Control. Conf. (ACC)* **2018-June**, 2814–2820, 10.23919/ACC.2018.8430866 (2018).

**95.** Suárez, L. E., Markello, R. D., Betzel, R. F. & Misic, B. Linking Structure and Function in Macroscale Brain Networks. *Trends Cogn. Sci.* **24**, 302–315, 10.1016/J.TICS.2020.01.008 (2020).

**96.** Yang, R., Sala, F. & Bogdan, P. Hidden network generating rules from partially observed complex networks. *Commun. Phys. 2021 4:1* **4**, 1–12, 10.1038/s42005-021-00701-5 (2021).

**97.** Xue, Y. & Bogdan, P. Reconstructing missing complex networks against adversarial interventions. *Nat. Commun. 2019 10:1* **10**, 1–12, 10.1038/s41467-019-09774-x (2019).

**98.** Churchland, M. M. *et al.* Neural population dynamics during reaching. *Nature* **487**, 51–56, 10.1038/nature11129 (2012).

**99.** Chandrasekaran, C., Peixoto, D., Newsome, W. T. & Shenoy, K. V. Laminar differences in decision-related neural activity in dorsal premotor cortex. *Nat. Commun. 2017 8:1* **8**, 1–16, 10.1038/s41467-017-00715-0 (2017).

**100.** Kaufman, M. T. *et al.* The largest response component in the motor cortex reflects movement timing but not movement type. *eNeuro* **3**, 85–101, 10.1523/ENEURO.0085-16.2016 (2016).

**101.** Clawson, W. *et al.* Computing hubs in the hippocampus and cortex. *Sci. Adv.* **5**, eaax4843, 10.1126/sciadv.aax4843 (2019).

**102.** Schroeder, K. E. *et al.* Disruption of corticocortical information transfer during ketamine anesthesia in the primate brain. *NeuroImage* **134**, 459–465, 10.1016/j.neuroimage.2016.04.039 (2016).

**103.** Kaufman, M. T., Churchland, M. M., Ryu, S. I. & Shenoy, K. V. Cortical activity in the null space: permitting preparation without movement. *Nat. neuroscience* **17**, 440, 10.1038/NN.3643 (2014).

**104.** Verbruggen, F. & Logan, G. D. Response inhibition in the stop-signal paradigm, 10.1016/j.tics.2008.07.005 (2008).

**105.** Schall, J. D., Palmeri, T. J. & Logan, G. D. Models of inhibitory control. *Philos. Transactions Royal Soc. B: Biol. Sci.* **372**, 20160193, 10.1098/rstb.2016.0193 (2017).

**106.** Wei, W., Rubin, J. E. & Wang, X. J. Role of the indirect pathway of the basal ganglia in perceptual decision making. *J. Neurosci.* **35**, 4052–4064, 10.1523/JNEUROSCI.3611-14.2015 (2015).

**107.** Drummond, N. M., Cressman, E. K. & Carlsen, A. N. Go-activation endures following the presentation of a stop-signal: evidence from startle. *J Neurophysiol* **117**, 403–411, 10.1152/jn.00567.2016.-It (2017).

**108.** Dunovan, K., Lynch, B., Molesworth, T. & Verstynen, T. Competing basal ganglia pathways determine the difference between stopping and deciding not to go. *eLife* **4**, 10.7554/ELIFE.08723 (2015).

**109.** Gu, Y., Qi, Y. & Gong, P. Rich-club connectivity, diverse population coupling, and dynamical activity patterns emerging from local cortical circuits. *PLoS Comput. Biol.* **15**, e1006902, 10.1371/journal.pcbi.1006902 (2019).

**110.** Perin, R., Berger, T. K. & Markram, H. A synaptic organizing principle for cortical neuronal groups. *Proc. Natl. Acad. Sci. United States Am.* **108**, 5419–5424, 10.1073/pnas.1016051108 (2011).

**111.** Schroeter, M. S., Charlesworth, P., Kitzbichler, M. G., Paulsen, O. & Bullmore, E. T. Emergence of rich-club topology and coordinated dynamics in development of hippocampal functional networks In vitro. *J. Neurosci.* **35**, 5459–5470, 10.1523/JNEUROSCI.4259-14.2015 (2015).

**112.** Gal, E. *et al.* Rich cell-type-specific network topology in neocortical microcircuitry. *Nat. Neurosci.* **20**, 1004–1013, 10.1038/nn.4576 (2017).

**113.** Hilgetag, C., O'Neill, M. A. & Young, M. P. Hierarchical organization of macaque and cat cortical sensory systems explored with a novel network processor. *Philos. Transactions Royal Soc. London. Ser. B: Biol. Sci.* **355**, 71–89, 10.1098/rstb.2000.0550 (2000).

**114.** Hilgetag, C. C. & Kaiser, M. Clustered organization of cortical connectivity, 10.1385/NI:2:3:353 (2004).

**115.** Felleman, D. J. & Van Essen, D. C. Distributed Hierarchical Processing in the Primate Cerebral Cortex. *Cereb. Cortex* **1**, 1–47, 10.1093/CERCOR/1.1.1-A (1991).

**116.** Sporns, O., Tononi, G. & Kötter, R. The Human Connectome: A Structural Description of the Human Brain. *PLoS Comput. Biol.* **1**, e42, 10.1371/journal.pcbi.0010042 (2005).

**117.** Kaiser, M. Hierarchy and dynamics of neural networks. *Front. Neuroinformatics* **4**, 112, 10.3389/fninf.2010.00112 (2010).

**118.** Zamora-López. Cortical hubs form a module for multisensory integration on top of the hierarchy of cortical networks. *Front. Neuroinformatics* **4**, 1, 10.3389/neuro.11.001.2010 (2010).

**119.** Zeki, S. & Shipp, S. The functional logic of cortical connections. *Nature* **335**, 311–317, 10.1038/335311a0 (1988).

**120.** Tononi, G., Sporns, O. & Edelman, G. M. A measure for brain complexity: Relating functional segregation and integration in the nervous system. *Proc. Natl. Acad. Sci. United States Am.* **91**, 5033–5037, 10.1073/pnas.91.11.5033 (1994).

**121.** Sporns, O., Honey, C. J. & Kötter, R. Identification and Classification of Hubs in Brain Networks. *PLoS ONE* **2**, e1049, 10.1371/journal.pone.0001049 (2007).

**122.** Watanabe, T. *et al.* Energy landscapes of resting-state brain networks. *Front. Neuroinformatics* **8**, 12, 10.3389/fninf.2014.00012 (2014).

**123.** Kaiser, M., Görner, M. & Hilgetag, C. C. Criticality of spreading dynamics in hierarchical cluster networks without inhibition. *New J. Phys.* **9**, 110, 10.1088/1367-2630/9/5/110 (2007).

**124.** Hilgetag, C. C. & Goulas, A. 'Hierarchy' in the organization of brain networks. *Philos. Transactions Royal Soc. B: Biol. Sci.* **375**, 20190319, 10.1098/rstb.2019.0319 (2020).

**125.** Fox, M. D. *et al.* The human brain is intrinsically organized into dynamic, anticorrelated functional networks. *Proc. Natl. Acad. Sci. United States Am.* **102**, 9673–9678, 10.1073/pnas.0504136102 (2005).

**126.** He, B. J. Scale-free properties of the functional magnetic resonance imaging signal during rest and task. *J. Neurosci.* **31**, 13786–13795, 10.1523/JNEUROSCI.2111-11.2011 (2011).

**127.** Zalesky, A., Fornito, A., Cocchi, L., Gollo, L. L. & Breakspear, M. Time-resolved resting-state brain networks. *Proc. Natl. Acad. Sci. United States Am.* **111**, 10341–10346, 10.1073/pnas.1400181111 (2014).

**128.** Cirillo, R., Fascianelli, V., Ferrucci, L. & Genovesio, A. Neural Intrinsic Timescales in the Macaque Dorsal Premotor Cortex Predict the Strength of Spatial Response Coding. *iScience* **10**, 203–210, 10.1016/J.ISCI.2018.11.033 (2018).

**129.** Shine, J. M. *et al.* The Dynamics of Functional Brain Networks: Integrated Network States during Cognitive Task Performance. *Neuron* **92**, 544–554, 10.1016/j.neuron.2016.09.018 (2016).

**130.** Vidaurre, D., Smith, S. M. & Woolrich, M. W. Brain network dynamics are hierarchically organized in time. *Proc. Natl. Acad. Sci. United States Am.* **114**, 12827–12832, 10.1073/pnas.1705120114 (2017).

**131.** Morcos, A. S. & Harvey, C. D. History-dependent variability in population dynamics during evidence accumulation in cortex. *Nat. Neurosci.* **19**, 1672–1681, 10.1038/nn.4403 (2016).